Electron momentum distributions in metals using the Angular Correlation of positron Annihilation Radiation (ACAR)

Name : Leung Wai Yan
UID: 2007132498
Course code:PHYS3531 Physics Project

Supervisors:
Prof. C. D. Beling
Department of Physics, HKU

Prof. S. Fung
Department of Physics, HKU

Contents

1 Introduction **3**
- 1.1 Early positron research . . . 3
- 1.2 Outline . . . 4

2 Background Theory **5**
- 2.1 Positron . . . 5
  - 2.1.1 Positrons - Antimatter of electrons . . . 5
  - 2.1.2 Electron–positron annihilation . . . 5
  - 2.1.3 Positron Sources . . . 6
- 2.2 Angular Correlation of Annihilation Radiation . . . 7
- 2.3 Fermi Gas Model . . . 9

3 Description of the Experiment **12**
- 3.1 1D ACAR Spectrometer . . . 12
  - 3.1.1 Components . . . 12
  - 3.1.2 Geometrical parameters . . . 12
- 3.2 Germanium-68 Source . . . 14
- 3.3 NaI(TI) Scintillation Detector . . . 14
  - 3.3.1 The photoelectric effect . . . 15
  - 3.3.2 Compton scattering . . . 15
  - 3.3.3 The Pair Production . . . 16
- 3.4 The photomultiplier tube . . . 17
- 3.5 Modular Electronics Instruments . . . 18
  - 3.5.1 High-Voltage power supply . . . 18
  - 3.5.2 Scintillation Preamplifier . . . 18
  - 3.5.3 Amplifier . . . 19
  - 3.5.4 Timing Single-Channel Analyzer . . . 19
  - 3.5.5 Universal Coincidence . . . 20
- 3.6 Data Acquisition Unit and Automated measurement . . . 21
  - 3.6.1 Multifunction Data Acquisition (DAQ) Card . . . 21
  - 3.6.2 Digimatic measuring gauge . . . 22
  - 3.6.3 Measurement data transfer device . . . 22
  - 3.6.4 LabVIEW Program . . . 23
    - 3.6.4.1 Data Structure . . . 23
    - 3.6.4.2 Procedures . . . 23
    - 3.6.4.3 Output . . . 24
- 3.7 Testing Materials . . . 24

4 Result and Data Analysis **25**
4.1 Aluminium . . . 26
4.1.1 ACAR Result . . . 26
4.1.2 Fermi-Energy Calculation . . . 28
4.1.3 Comparison with Fermi-gas model . . . 28
4.2 Copper . . . 29
4.2.1 ACAR Result . . . 29
4.2.2 Comparison with Fermi-gas model . . . 31
4.3 Stainless Steel . . . 32
4.3.1 ACAR Result . . . 32
4.3.2 Fermi-Energy Calculation . . . 33
4.3.3 Comparison with Fermi-gas model . . . 33

5 Discussion **34**
5.1 ACAR observation . . . 34
5.2 Tuning the equipments . . . 34
5.2.1 This Year and Last Year . . . 34
5.2.2 Problems related to the Modular Electronics Instruments . . . 35
5.2.3 Problems related to the ACAR Setup . . . 37
5.2.4 Problems related to the Data Acquisition Units . . . 37
5.3 Programing . . . 39
5.3.1 LabVIEW Programs . . . 39
5.3.2 C++ Programs . . . 39
5.3.3 GNU Plot . . . 40
5.4 Improvement . . . 40
5.4.1 Extending the range of motor . . . 40
5.4.2 Stronger Positron Source . . . 40
5.4.3 Better Remote control . . . 40

6 Conclusion **41**

A Data Acquisition Program **45**

B Data Analysis Program and Scripts **48**

C GNU Plot fitting logs **55**

Chapter 1

Introduction

Positron, the anti-matter of electron, has been used in laboratories, medical centers and industrial research facilities for several decades. It can be naturally formed through beta-decay or by pair productions through high energy collision. In laboratories, positrons are often generated by radioactive sources. Among all the anti-matters, it is often used in research as it is most available than other anti-matters. It is one of the handy tools for scientists to investigate the fundamental physics law and the study of matter. There are many new techniques for creating and manipulating positrons and scientists utilize positrons and study the scattering of positrons.

1.1 Early positron research

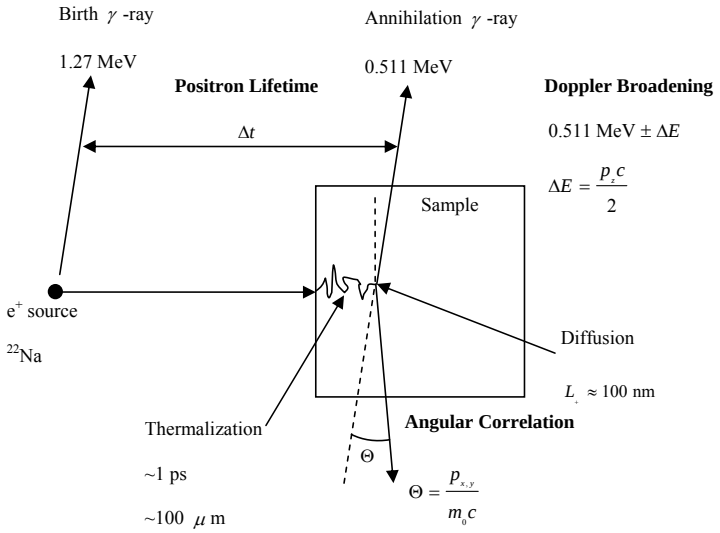

Figure 1.1: Schematic diagram of various positron research [2]

There are several types of positron experiments. Slow positrons are often generated in the isotope source, and they are directed to penetrate the sample. Thermalization occurs with in a few picoseconds and the positrons diffuse before it annihilates[7]. The positron life time experiment measures the difference between the time when the birth-ray detected and the annihilation gamma ray detected. The Doppler Broadening Spectroscopy(DBS) records the broadening in energy spectrum of the annihilation gamma

ray.[7]The Angular Correlation of positron Annihilation Radiation(ACAR) records the angular deviation from 180^o of the gamma ray pairs. The last two experiment type is very similar as they use the fact that the electron momentum is non-zero and it leads to energy difference and momentum difference in the two annihilation ray[7].

The development of the Angular Correlation of positron Annihilation Radiation (ACAR) technique in research has taken several decades. The first measurement of this technique is carried out by DeBenedetti, Konneker, Primakoff and Cown in 1949, using Gold(Au) as the testing material[8]. Afterwards, various of substances have been observed using this technique such as metals, ionic salts and several insulators by various scientists [8]. In 1977, Berko, Mader and Haghooie first announced the use of two-dimensional angular correlation of annihilation (2D ACAR) on a metal [5].

1.2 Outline

Experiments with ACAR technique require a general gamma-gamma coincidence electronic setup. It involves the coincidence of a pair of gamma-ray signals from the annihilated positron and electron. Thus, the basic function of the electronics in this experiment is to collect the radiation events. The scintillation detector grabs the radiation signals and passed to a series of electronics for 1) Amplifying the signal, 2) Filtering the signal and 3) Coincident the signal with another detector. Thus, a pair of setup is required for coincidence and pulses from two detectors have to produce their pulses and overlap in time such that a coincidence happenes. A counter will do the job of counting the events of coincidence.

The angular correlation means this experiment is related to an angle. Specifically, it is the angle between the annihilation gamma ray that matters. For a pair of stationary particles annihilation, the angle of each annihilation gamma ray will be exactly 180^o for the conservation of linear momentum. Any derivation from this angle is the effect of momentum present in the particle. In some metals and semimetals, positrons will be slowed down in the lattice of the polycrystalline material and annihilation often occurred in free state[4]. Therefore the addition momentum in angular correlation experiment can be regarded as the momentum of electrons inside the lattice before the annihilation.

Thus, the ACAR experiment technique helps the study of electron momentum distribution. As we shall see, any break in the distribution could determine the shape and size of the Fermi surface. In quantum mechanics, a particle can be described by a wave function. When the wave function is described in the momentum space by Fourier transform, the probability of getting an electron with certain momentum is directly proportional to the square of the amplitude. Obtaining a certain angle between the annihilation photons also depends on the positron-electron wave function in momentum space [4].

In this report, the related theory will be discussed in the next chapter and followed by the details of the experiment. The result of the ACAR experiments will be presented graphically and the discussion will cover the explanation of experimental results, the error in the experiments and difficulties encountered in this experiment.

Chapter 2

Background Theory

2.1 Positron

2.1.1 Positrons - Antimatter of electrons

The prediction of antiparticle of electron was done by Paul. A.M. Dirac in 1930 [1]. When his Lorentz invariant formulation of the electron was developed, he noted that the following relativistic energy equation has a negative energy solution which has real physical significances[1].

$$E^2 = m^2c^4 + p^2c^2 \tag{2.1}$$

Therefore, he postulated that there exists a sea of electrons with energy level between $-mc^2$ and $-\infty$ that has been fully occupied according to the Pauli Exclusion Principle, and those electrons are not observable with any means[1]. However, he soon realized this is not the case and his theory was actually predicted a new particle which has the same rest mass as electron but with opposite charge[1]. The first discovery of positron was by Anderson on 1933 in a cloud chamber where he studied the cosmic radiation[1]. Later, the existence of positrons and the pair production was confirmed and observed by Blackett and Occhialini in 1933[1]. A positron has exactly the same mass and lifetime as an electron[1]. They are usually obtained from the β^+decays of radioactive nucleus in the laboratory.

2.1.2 Electron–positron annihilation

The electron $e^-$and positron e^+ is a matter-antimatter pair, they will annihilate if they collide with each other and change their mass constituents into energy. The annihilation of electron and positron will create gamma ray photons or other particles[1]. Positron is a stable particle in vacuum and has a theoretical lifetime which equals to electron. However, normal matter contains electrons that will annihilate with a positron, thus the lifetime is inversely proportional to the density of local electron[1].

The annihilation of a positron with an electron may proceed in different mechanisms. The annihilation process may give out one gamma, two gamma or three gamma rays, the positron can also annihilate with the inner shell electrons which excite the nuclei rather than giving out radiation[1]. Usually, the equation for the electron-positron annihilation is simply like this:

$$e^- + e^+ \rightarrow 2\gamma \tag{2.2}$$

Two gamma rays are formed to conserve the linear momentum. Each gamma ray carries an energy of $511keV$, which is the rest energy of an electron or a positron.

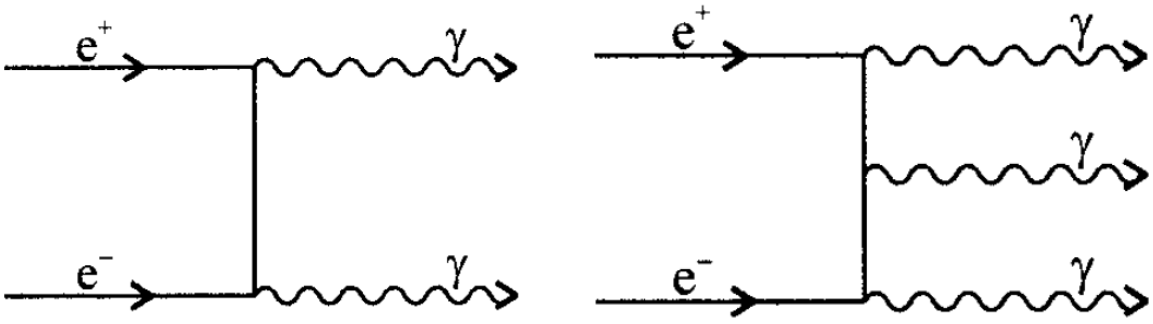

Figure 2.1: Feynman Diagram showing e^+e^-Annihilation with the emission of 2 gamma rays (Left); Feynman Diagram showing e^+e^-Annihilation with the emission of 3 gamma rays (Right) [1].

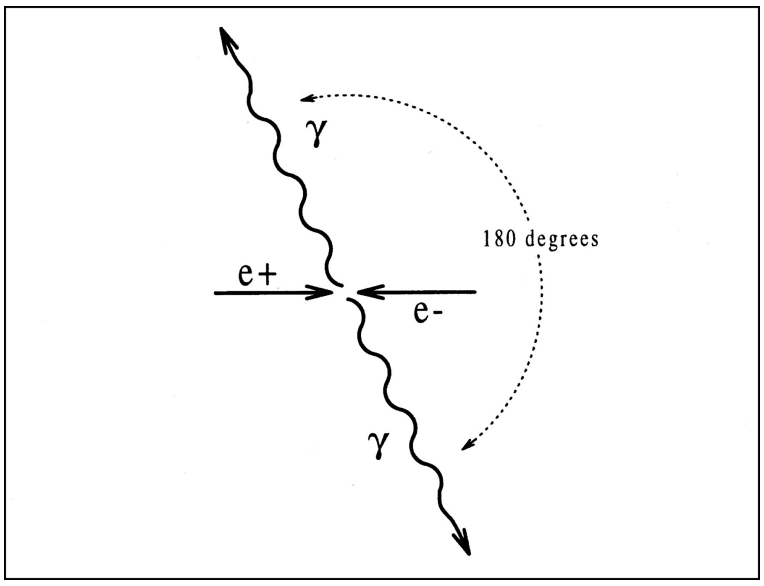

Figure 2.2: Diagram of electron-positron annihilation, producing two 511 keV photons leaving in opposite directions.

2.1.3 Positron Sources

There are several ways to get the positrons. For high-flux positron facilities, positrons are obtained by pair production.

The positron source used in this project is the Germanium-68 (^{68}Ge). The half-life of ^{68}Ge was found to be 275 days, which is relatively stable among the radioisotopes of Germanium[3]. According to the decay scheme shown in Figure 2.3, 100% of the Germanium-68(^{68}Ge) first decays to Gallium-68(^{68}Ga) by electron capture, the atomic number is increased by one. ^{68}Ga has a half life of 68 minutes, and the unstable ^{68}Ga then decays by the following pathways:

1. 84% of ^{68}Ga decays by positron emission to stable Zinc-68(^{68}Zn).
2. 3.5% of ^{68}Ga decays by positron emission to excited Zinc-68($^{68}Zn*$) and carried out by a photon emission of $1.02keV$.

3. 9.8% of ^{68}Ga decays by electron capture to stable Zinc-68(^{68}Zn).

4. 3.9% of ^{68}Ga decays by electron capture to excited Zinc-68($^{68}Zn*$) and carried out by a photon emission of $1.02keV$.

For our interested pathways:

$$^{68}Ge + e^- \rightarrow {}^{68}Ga + \tilde{\nu_e} \tag{2.3}$$
$$^{68}Ga \rightarrow {}^{68}Zn + e^+ + \nu_e \tag{2.4}$$
$$^{68}Ga \rightarrow {}^{68}Zn* + e^+ + \nu_e \rightarrow {}^{68}Zn + \gamma + e^+ + \nu_e \tag{2.5}$$

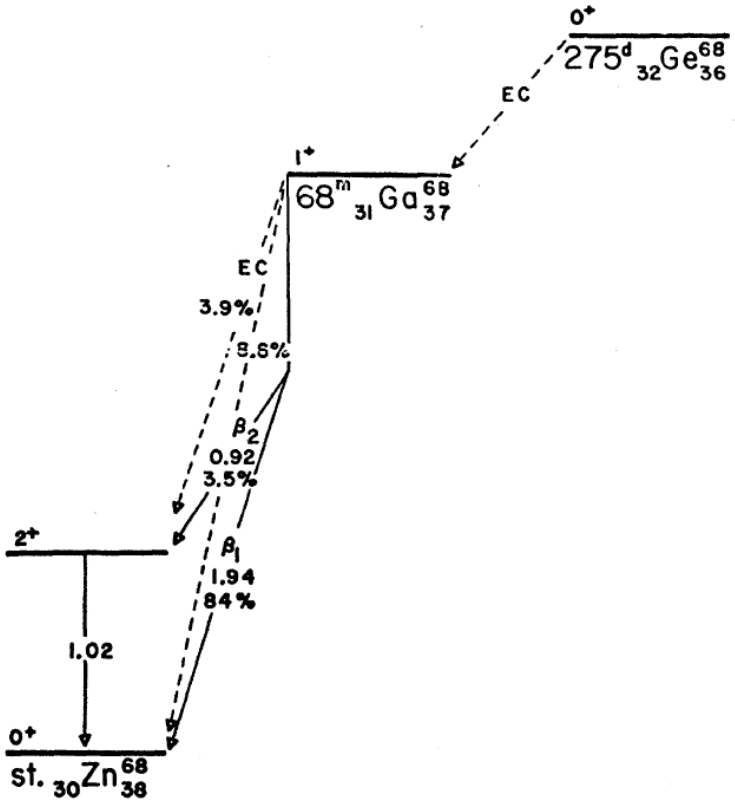

Figure 2.3: Decay Scheme for ^{68}Ge [3]

2.2 Angular Correlation of Annihilation Radiation

In condensed matter, the positron annihilation is dominant by 2γ process and the positron is thermalized[5]. The energy and momentum, undoubtedly, is conserved during the annihilation. In the center-of-mass frame, the two annihilation gamma ray emerged from the position of annihilation in exactly opposite direction[5]. Each of them carries half of the total energy $2m_0c^2$, where m_0 is the rest mass of electron (or positron). In the laboratory frame, the situation becomes complicated since the electron has a small but not negligible momentum (The thermalized positron also has a small amount of momentum). We assume the mean photon emission axis be the z-axis and the x,y axis are set such that y-axis is pointing upward. The deviated gamma ray leaves with an angle α with the line parallel to another gamma ray.

The z component of the additional momentum causes a Doppler shifting effect to the two gamma ray[5]. Which is equal to

$$\Delta E = \pm c p_z/2 \tag{2.6}$$

The perpendicular components (x and y) gives a small angular deviation from anti parallelism(WEST),

$$\alpha = \frac{\sqrt{p^2 - p_z^2}}{m_0 c} \tag{2.7}$$

For small angle θ and ϕ, we have

$$\theta = \frac{p_z}{m_0 c} \tag{2.8}$$

$$\phi = \frac{p_y}{m_0 c} \tag{2.9}$$

The 1D ACAR instrument only sensitive to the x-component of the momentum as we have a much broader vertical resolution than the observed angular distributions[8].

In polycrystalline materials, the result will be "an average over all orientations of the crystal structure with respect to the apparatus"[8]. The distribution in the x component of momentum $N_x(p_x)$ and the distribution in the magnitude of momentum are related by this equation:

$$N_x(p_x) = \frac{1}{2}\int_{p_x}^{\infty} \frac{N(p)}{p} dp \tag{2.10}$$

This simple model assumed that the valence electrons in metal behave as a Fermi gas. With "the approximation of zero temperature", the distribution in the magnitude of momentum are expressed as

$$\begin{aligned} N(p) &= p^2 \quad \text{for} \quad p^2 < p_F^2 \\ &= 0 \quad \text{for} \quad p^2 > p_F^2 \end{aligned} \tag{2.11}$$

where $p_F$is the Fermi momentum and the discussion will be in the next section. Assume that the momentum of thermalized positron is negligible and the annihilation probability is independent of the electron momentum, the distribution in the x component of momentum are expressed as

$$\begin{aligned} N_x(p_x) &= (p_F^2 - p_z^2) \quad \text{for} \quad p^2 < p_F^2 \\ &= 0 \quad \text{for} \quad p^2 > p_F^2 \end{aligned} \tag{2.12}$$

which has a form of inverted parabola[8].

Thus the root of the distribution in the x component of momentum will gives the Fermi momentum of the material.

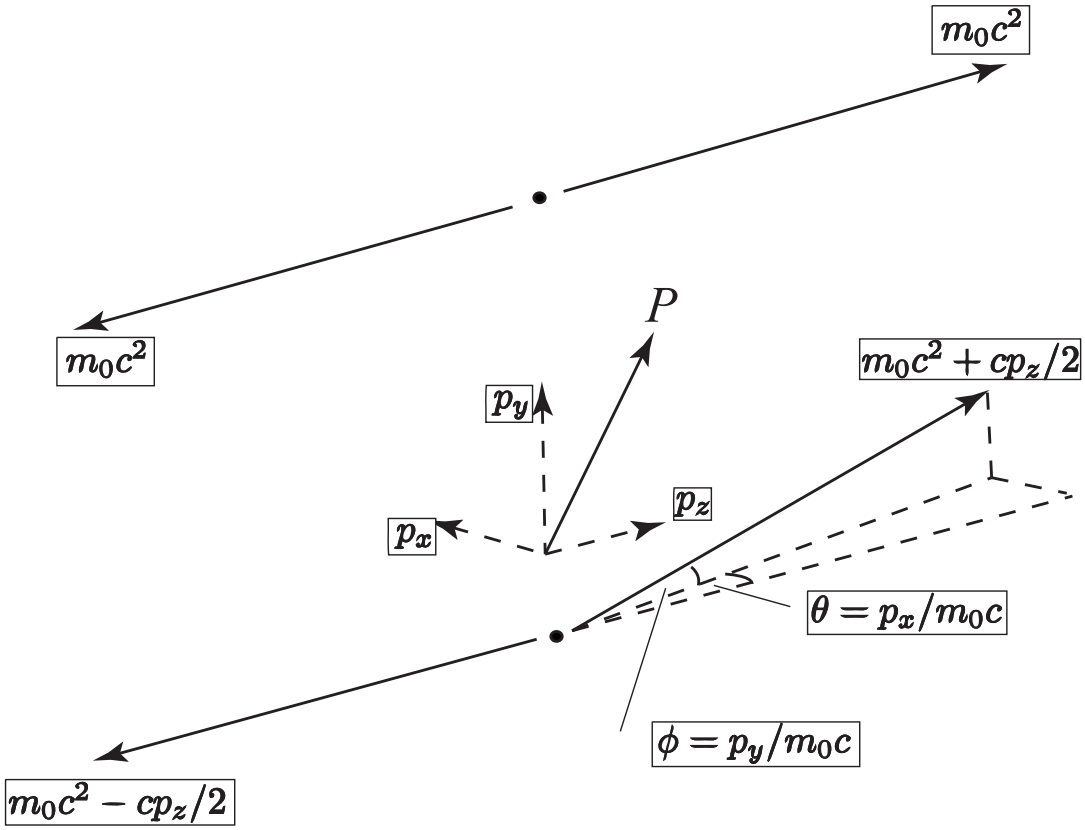

Figure 2.4: 2γ annihilation (Up) In the center-of-mass frame (Down) In the laboratory frame [5]

2.3 Fermi Gas Model

In Quantum mechanics, the Pauli Exclusion principle states that two identical fermions cannot occupy the same quantum state. We shall see that this principle has a profound impact to our world. Electron is a fermion with spin $1/2$. As there is a huge amount of electrons in the metal lattice, the energy and momentum of the electrons can be formulated by the Fermi gas model, which describes the behavior of a sea of electrons in vacuum.
We consider N fermions with spin $1/2$ that do not interacts with each other and the N fermions are subjected to an infinite well potential. In one dimension, the problem can be solved by considering the time independent Schrodinger equation of the 1D infinite square well with length L:

$$-\frac{\hbar^2}{2m}\frac{\partial^2\psi}{\partial x^2} = E\psi \tag{2.13}$$

which can be solved analytically and the eigenfunction is found to be:

$$\psi_n(x) = \sqrt{\frac{2}{L}}\sin\frac{n\pi x}{L} \tag{2.14}$$

with eigenenergies

$$E_n = \frac{\hbar^2\pi^2}{2mL^2}n^2 \tag{2.15}$$

.
In three dimension, the problem can be solved by considering the time independent Schrodinger equation of the 3D box with sides L:

$$-\frac{\hbar^2}{2m}\nabla^2\Psi = E\Psi \tag{2.16}$$

The calculation is straightforward as we can let the wave function be a separable function:

$$\Psi(x,y,z) = X(x)Y(y)Z(z) \tag{2.17}$$

And the partial differential equation becomes

$$-\frac{\hbar^2}{2m}\left(\frac{\partial^2}{\partial x^2}+\frac{\partial^2}{\partial y^2}+\frac{\partial^2}{\partial z^2}\right)XYZ = EXYZ \tag{2.18}$$

And simplify, we get

$$\left(-\frac{\hbar^2}{2m}\frac{1}{X}\frac{\partial^2 X}{\partial x^2}\right)+\left(-\frac{\hbar^2}{2m}\frac{1}{Y}\frac{\partial^2 Y}{\partial y^2}\right)+\left(-\frac{\hbar^2}{2m}\frac{1}{Z}\frac{\partial^2 Z}{\partial z^2}\right) = E \tag{2.19}$$

By letting $E = E_x + E_y + E_z$, we have

$$-\frac{\hbar^2}{2m}\frac{\partial^2 X}{\partial x^2} = E_x X \;\; -\frac{\hbar^2}{2m}\frac{\partial^2 Y}{\partial y^2} = E_y Y \;\; -\frac{\hbar^2}{2m}\frac{\partial^2 Z}{\partial z^2} = E_z Z \tag{2.20}$$

Which is identical to three 1D infinite square well problem. And applying the above result, we have:

$$\begin{aligned}\Psi(x,y,z) = XYZ &= \sqrt{\frac{2}{L}}\sin\frac{n_1\pi x}{L}\sqrt{\frac{2}{L}}\sin\frac{n_2\pi y}{L}\sqrt{\frac{2}{L}}\sin\frac{n_3\pi z}{L} \\ &= \left(\frac{2}{L}\right)^{3/2}\sin\frac{n_1\pi x}{L}\sin\frac{n_2\pi y}{L}\sin\frac{n_3\pi z}{L}\end{aligned} \tag{2.21}$$

with eigenenergies

$$E = \frac{\hbar^2\pi^2}{2mL^2}\left(n_1^2+n_2^2+n_3^2\right) \tag{2.22}$$

To solve the problem of N fermions in the 3D box, we would like to know how the fermions are filled up with the combinations of (n_1,n_2,n_3) such that the amount of energy is minimum. Or, we would like to find a number E_F, such that the energy of different combination of (n_1,n_2,n_3) is smaller than E_F, and the total energy of the system will be smaller than NE_F.
We can consider (n_1,n_2,n_3) as the x,y,z coordinate of a three dimensional space. If N is very large, it is a good approximation that (n_1,n_2,n_3) must lie inside a sphere of radius R, where

$$n_1^2+n_2^2+n_3^3 = R^2 = \frac{2mL^2E_F}{\hbar^2\pi^2} \tag{2.23}$$

Then, N will be the total number filled in the octant of the sphere (where $n_1,n_2,n_3 > 0$), or the volume of the octant of the sphere. Thus N can be expressed as

$$\frac{1}{8}\left(\frac{4}{3}\pi R^3\right) = \frac{1}{8}\left(\frac{4}{3}\pi(R^2)^{3/2}\right) = \frac{1}{8}\left(\frac{4}{3}\pi\left(\frac{2mL^2E_F}{\hbar^2\pi^2}\right)^{\frac{3}{2}}\right) \tag{2.24}$$

As each spin $1/2$ fermions have up and down state, thus

$$N = \frac{\pi}{3} L^3 \left(\frac{2mE_F}{\hbar^2 \pi^2} \right)^{\frac{3}{2}} \tag{2.25}$$

Since the number of fermions are proportional to the volume of the box L^3, thus let the number density be $n = \frac{N}{L^3}$, then by rearranging the above equation, we have

$$E_F = \frac{\hbar^2 \pi^2}{2m} \left(\frac{3n}{\pi} \right)^{\frac{2}{3}} \tag{2.26}$$

we called it the Fermi energy, which is defined as "the topmost filled level in the ground state of the N electron system"(Kittel). Also, in the momentum space, the energy is defined as

$$E = \frac{\hbar^2 k^2}{2m} \tag{2.27}$$

where k is the wave number and $p = \hbar k$. The "Fermi-wave number" that is defined by

$$E_F = \frac{\hbar^2 k_F^2}{2m} \tag{2.28}$$

And

$$p_F = \hbar k_F \tag{2.29}$$

which is called the "Fermi momentum", can also be defined.

Chapter 3

Description of the Experiment

3.1 1D ACAR Spectrometer

3.1.1 Components

The mechanical setup consists of the following components:

1. A fixed platform and a movable platform that can rotate about a vertical axis at the center.
2. Two movable trolleys sit on a pair of trails that are fixed on the platforms.
3. Two mounts inserted with scintillators, each behind two movable lead blocks.
4. A turntable placing sources and samples at the center of the setup.
5. A motor that drives the movable platforms to the left or right.
6. A mounted digimatic measuring gauge measure the movement of the movable platform.

3.1.2 Geometrical parameters

The Scintillation detectors are fixed on a movable slide that can move forward and backward along the rails. The distance between the detector and the sample can be set from $48.2 \pm 0.05cm$ to $100 \pm 0.05cm$. The width of the narrow opening of each detector is from $0cm$ to $4.6 \pm 0.05cm$.

Detector-detector distance $180cm \pm 0.05cm$

Detector-source distance $90cm \pm 0.05cm$

Gauge-source distance $70cm \pm 0.05cm$

Narrow-opening width $2mm \pm 0.05mm$

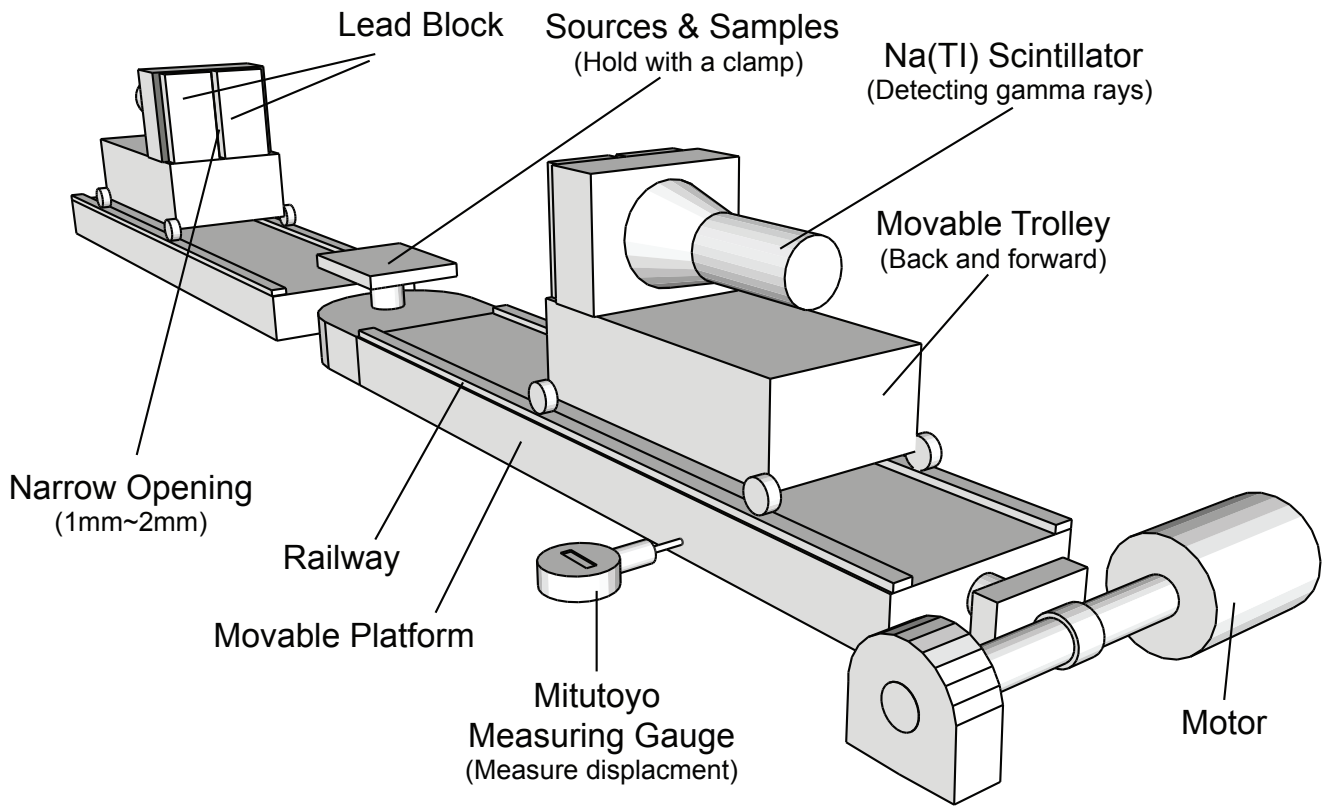

Figure 3.1: Schematic Diagram for the ACAR spectrometer

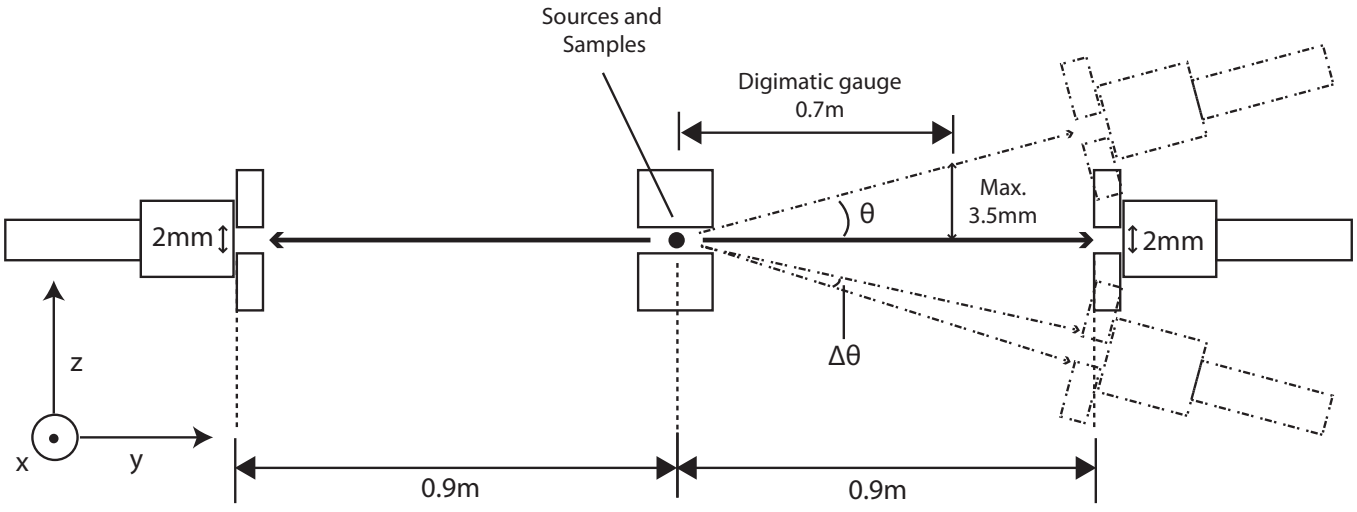

Figure 3.2: Schematic diagram for the 1D ACAR spectrometer and the critical geometrical parameters

3.2 Germanium-68 Source

The Germanium-68 source has been ordered from Eckert & Ziegler Isotope Products for this experiment. The data of the Source is as follows[11]:

Chemical nature Evaporated Ge-68 salts

Activity $100\mu Ci(3.7MBq)$

Reference Date 1st Feb 2010

Package Diameter $12.7mm$

Active Diameter $5.08\ mm$

Cover Kapton

The Ge-68 positron source is sealed inside kapton film with an extremely small thickness. It is sandwiched between two pieces of samples with identical thickness and material. The samples are tightened up such that the Ge-68 positron source is "stick" tightly on both surfaces. The positron emitted from the Ge salts will passed through the thin polymide film and go directly to the test materials. Only a small amount of radiation is absorbed by the kapton film. The gamma ray produced after annihilation with the electrons in the sample will be emitted from the gap between the samples or passed through the sample without significant loss in number.

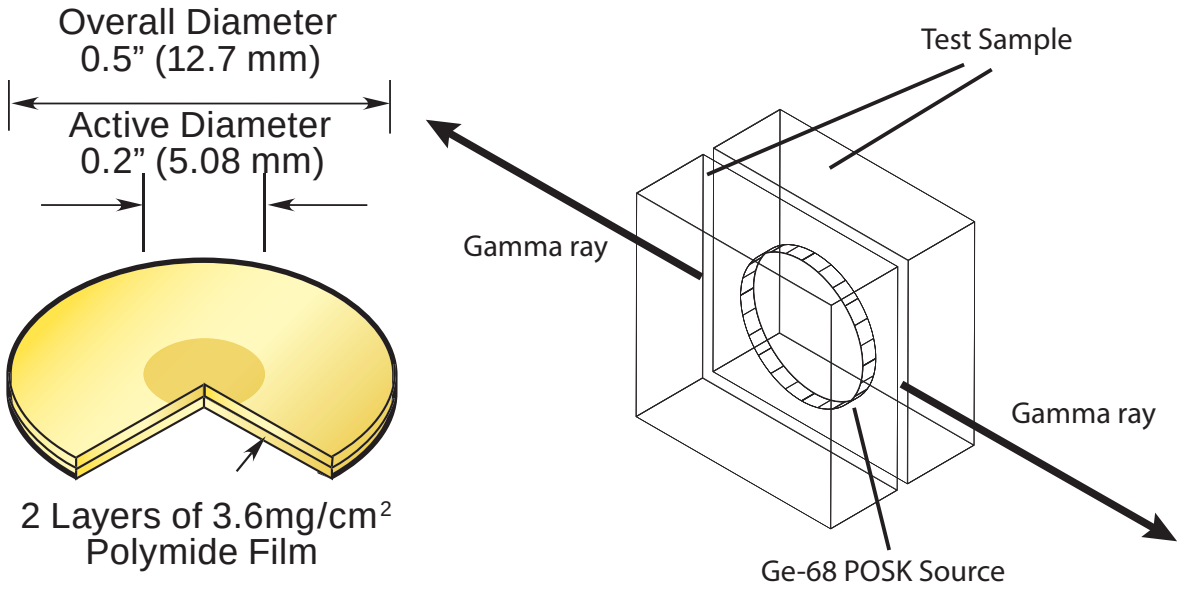

Figure 3.3: Left: Ge-68 POSK Configuration[11]; Right: Sources and Sample

3.3 NaI(TI) Scintillation Detector

In 1948, Robert Hofstadter discovered that when a trace amount of Thallium (Tl) was added into a crystal of Sodium Iodide (NaI), a large scintillation phenomenon were observed, then the alkali halide crystal,

NaI(Tl), has started to use in a scintillation detector [12]. The interaction of gamma-ray with atoms are important to understand the scintillation process. Since the typical energy of a gamma-ray is greater than the binding energy of an electron inside materials, the gamma-rays have excess energy to ionize matter [12]. There are three main mechanisms for the interaction:

1. The photoelectric effect
2. Compton scattering
3. Pair production

3.3.1 The photoelectric effect

In the photoelectric process, the incident gamma-ray photon will give its entire energy to a bound electron. The energetic electron is ejected from the atom, as a result, a vacancy formed in the atomic structure and it will remain in such an excited state for a short period[12]. Any electrons from a higher energy state will replace the vacancy such that the atom can achieve its lowest energy state[12]. A photon, as a result, is released when the electrons change state and the amount of energy released is exactly the amount of energy gap between the initial and final states. The amount of energy corresponds to X-ray spectrum, and the x-ray photon will be reabsorbed by outer shell electrons before it can leave the atom[12]. This is called an Auger electron which has enough energy to leave the atom[12]. Other electrons will filled the vacancies and emit additional characteristic X-rays and Auger electrons.

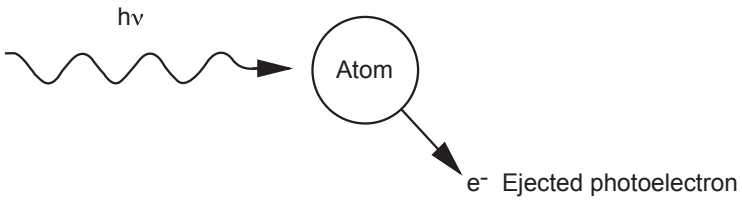

Figure 3.4: The photoelectric effect(WILKINSON)

3.3.2 Compton scattering

In Compton scattering, an electron is scattered by a photon (like a particle) that entered the crystal lattice [12]. The energy will be distributed between the electron and incident photon. If there is energy remained in the photon, it will still available for other scattering events and a final photoelectric event [12].

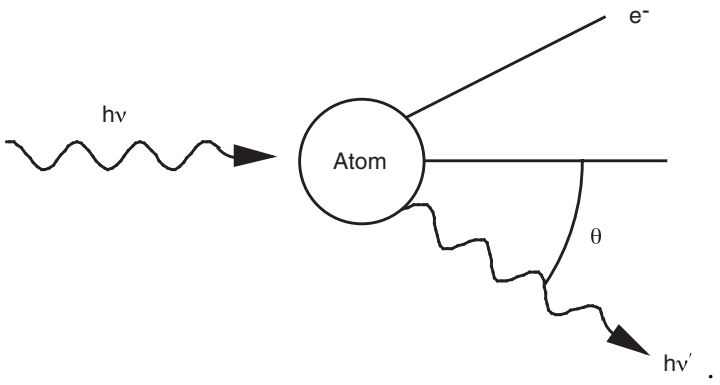

Figure 3.5: The Compton scattering(WILKINSON)

3.3.3 The Pair Production

Pair production can occur when the incident gamma-ray photon has energy exceeding the total rest mass energy of electron and positron(two times the rest mass energy of electron). An electron and a positron will be produced using the entire energy of the photon in the presence of Coulomb field produced by the nucleus. Energy is conserved in the following way:

$$E_{e^-} + E_{e^+} = h\nu - 2m_0c^2$$

The positron will then annihilate with electrons in matter, produce two 511 keV photons emitted in coincidence with an angle difference of 180°.

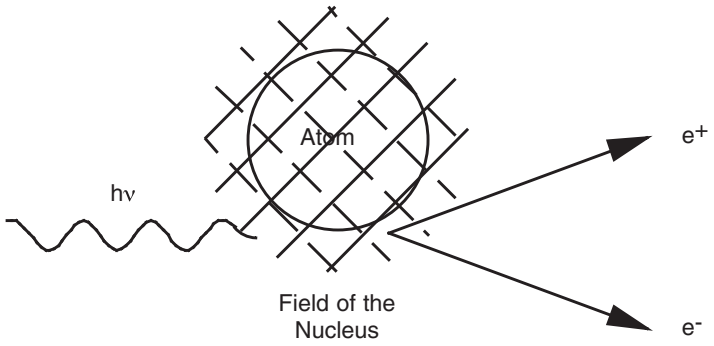

Figure 3.6: The Pair Production(WILKINSON)

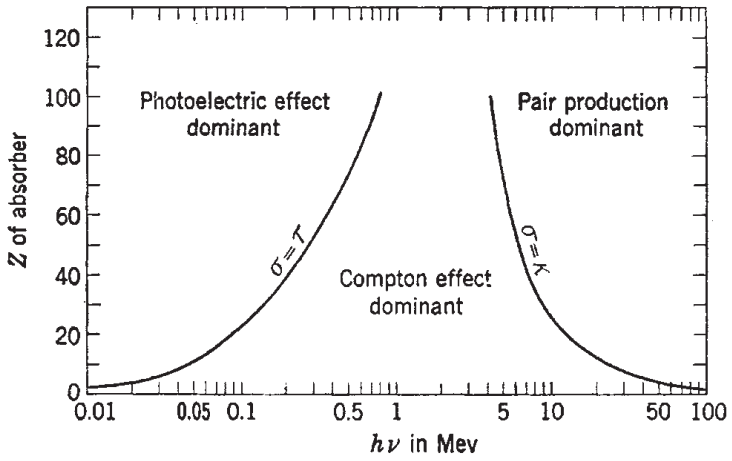

Figure 3.7: Three interaction mechanisms for different energy gamma-ray(WILKINSON)

3.4 The photomultiplier tube

When the NaI(TI) generate a weak scintillation pulse, the pulse of light will be converted to electric signal thought the photomultiplier tube. The tube converts light signals which consist of only a few hundred photons into a clean current pulse without adding a lot of random noice to the signal[10].There is a photocathode, a focusing electrode, and 10 or more dynodes inside the photomultiplier tube[6]. The photocathode consists of photoemissive material which absorbs the incident photon and its energy is transferred to an electron. Then the electron migrates to the surface and escape the surface of the photoemissive material[6]. Then the escaped electron are accelerated and strike the surface of one of the dynode. More than one electron will be emitted from the surface and they strike another dynode[6]. As a result, the number of electrons increases such that the amount of electron is enough for a current pulse[10].

3.5 Modular Electronics Instruments

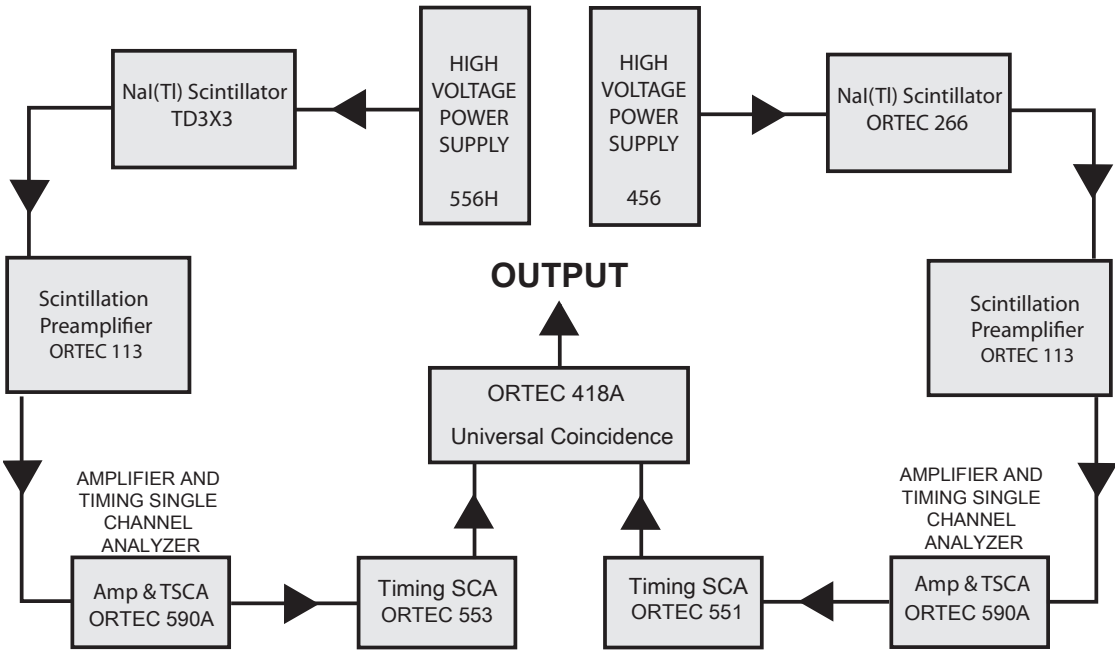

Figure 3.8: Schematic Diagram for electronics connection

3.5.1 High-Voltage power supply

A high voltage is necessary for the operation of the photomultiplier tube in the NaI Scintillation detectors.

Left Detector Model Ortec 556H ($0.6V$)

Right Detector Model Ortec 456 ($0.6V$)

In order to prevent overloading of the photomultiplier tube, the voltage should be lower than the maximum voltage output $\pm 3kV$.

3.5.2 Scintillation Preamplifier

Model Ortec 113

The main use of a preamplifier is to extract the signal from the scintillation detector before the noice accumulate significantly to degrade the quality of the signal[10]. The preamplifier is placed as near as possible to the detector. The Scintillation Preamplifier receive the anode signals from photomultiplier tubes. The charge in the photomultiplier output pulse is integrated on the input capacitance of the preamplifier to produce a voltage pulse[10]. A diode network prevents destruction of the input transistor if a sudden positive or negative high voltage is applied to the input[10]. The input capacitance is set to be Ω.

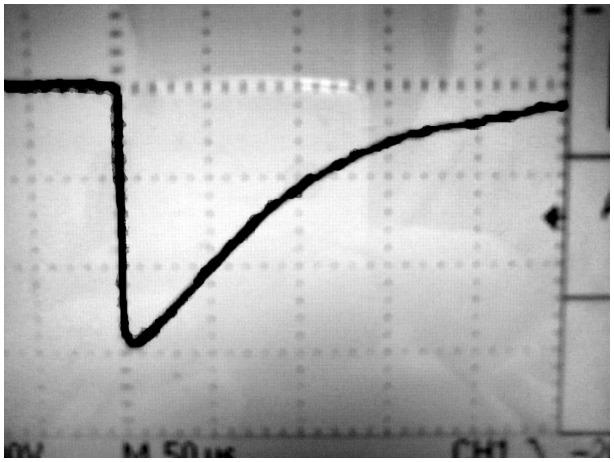

Figure 3.9: Signal coming out from the Scintillation Preamplifier(2V, 50μs)

3.5.3 Amplifier

Model Ortec 590A

The preamplifier is connected to the amplifier. It contains a low-noise shaping amplifier that employs active-filter shaping on the incoming signal[10]. The output has a unipolar semi-Gaussian pulse shape which is used for spectroscopy in systems[10]. The input capacitance is set to be Ω.

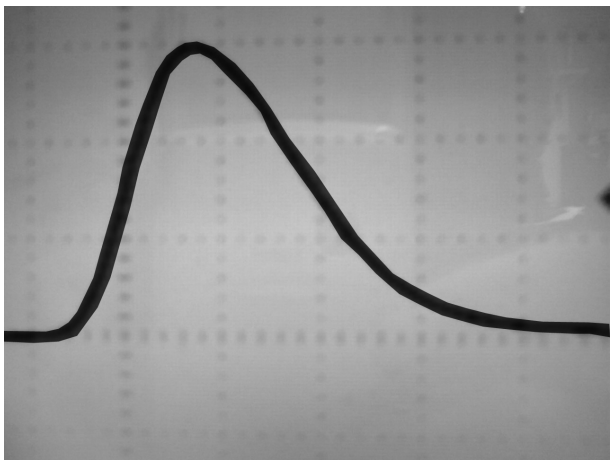

Figure 3.10: Signal coming out from the Amplifier (2V, 5μs)

3.5.4 Timing Single-Channel Analyzer

Model Ortec 551

The amplifier is connected to the timing single-channel analyzer. It is known that the amplifier will generate an analog pulse whose amplitude depends on the charge released in the detector[10]. The charge released is also proportional to the energy of the incident gamma-ray. Therefore, the signal whose energy we are interested can be selected by the range of signal levels at the output with the use of single-channel analyzers[10]. Logic pulses will be generated only if the peak of the input signals falls within the pulse height window that is constrained by two threshold levels. in the diagram below, we can see that there

are three pulses provided from the amplifier. Only B pulse will trigger a logic pulse as its peak falls into the window[10]. A pulse is lower than the window while C pulse exceeds the window, both pulses will not give a logic signal.

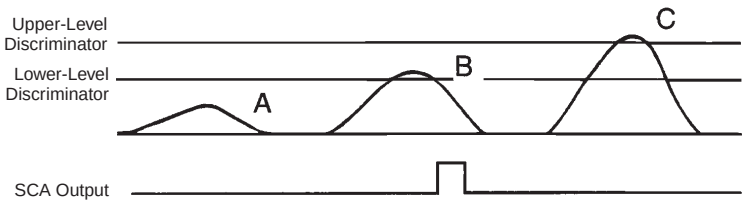

Figure 3.11: Signal selection through Single-Channel Analyzer[10]

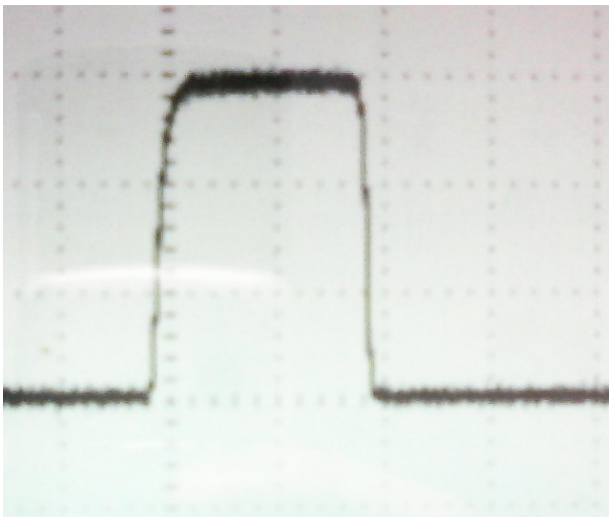

Figure 3.12: Signal coming out from the Single-Channel Analyzer (2V, 250*ns*)

3.5.5 Universal Coincidence

Model Ortec 418A

The timing single-channel analyzers on both sides are connected to the Universal Coincident Unit. A coincident unit will generate a logic pulse if a signal from one of the inputs arrived within the resolving time of a pulse from another input.

Figure 3.13: Coincident requirement[10]

3.6 Data Acquisition Unit and Automated measurement

3.6.1 Multifunction Data Acquisition (DAQ) Card

The multifunction data acquisition (DAQ) devices of National Instruments can provide analog input and output, digital input and output, and counter/timer circuitry. Only the counter function is used in this project and the counts are measured using the internal counter of the multifunction data acquisition card. The inner core of the coaxial cable is connected to the channel 42 (CTR 1 SRC) and the surface of the coaxial cable is connected to the channel (D GND) for grounding.

Model NI PCI-MIO-16E-4/NI PCI-6040E

Max Source Frequency 20MHz

Minimum Pulse Width 10ns

Timebase Stability 100ppm

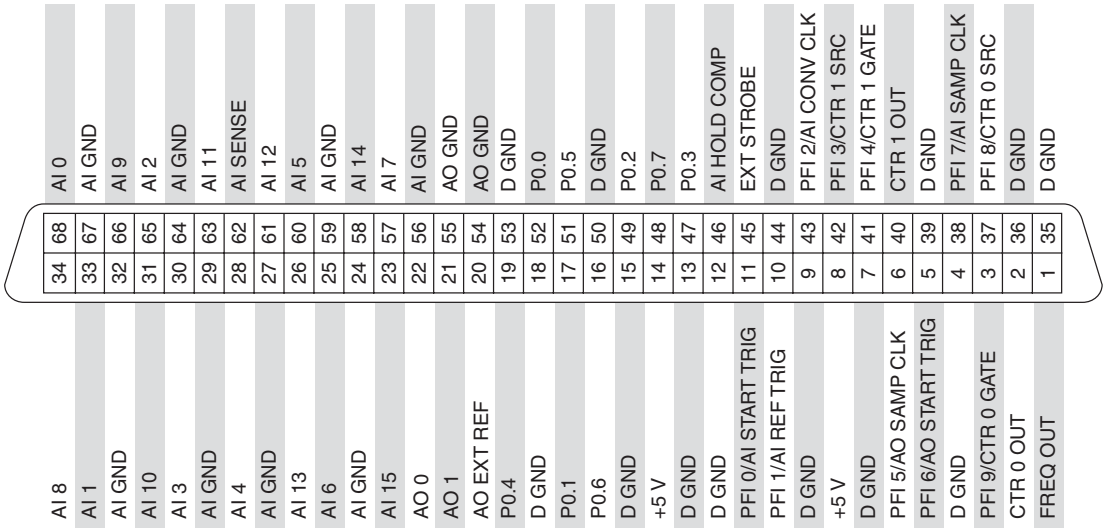

Figure 3.14: I/O Connector diagram for 16-Channel E Series DAQ device

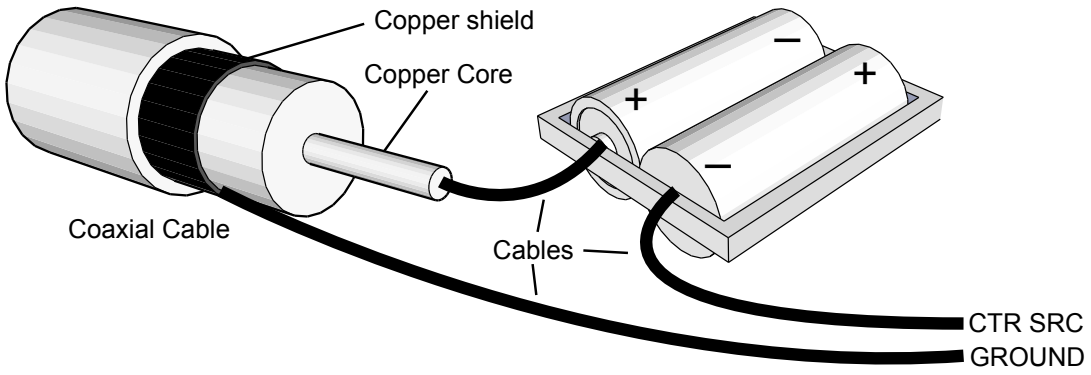

Figure 3.15: Connection diagram of the coaxial cable and the DAQ device

We have connected the signal to a negative voltage(-3V) generated by the battery such that the background noise are not passed and do not trigger the counter. The output pulse have a peak voltage 6V such that it is not filtered by the negative voltage.

3.6.2 Digimatic measuring gauge

Model Mitutoyo ID-C125MB

Stem ϕ 8mm

Resolution 0.0005" / 0.001 mm

Range 1" / 25.4 mm

Accuracy 0.00012"

Measuring Force 1.8N or less

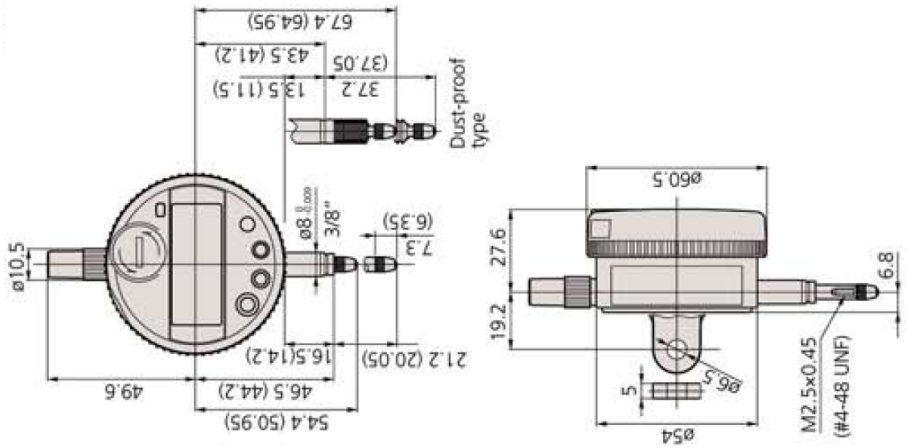

Figure 3.16: Digimatic Measuring Gauge (1"/25.4mm range model)(Mitutoyo Cat)

3.6.3 Measurement data transfer device

This device is a measurement data transfer device, which converts data from the measuring gauge into an RS-232 format and output the data via the RS-232 interface. When the computer sends a command (in ASCII) through COM port to the multiplexer, the multiplexer will return the digital reading (Also in ASCII) in the measuring gauge back to the computer.

Model Mitutoyo Multiplexer-10F

Connection RS-232

Baudrate 19,200

Communication method Half duplex

Start bit 1 bit

Data bit 8 bits(7-bit ASCII)

Stop bit 1 bit

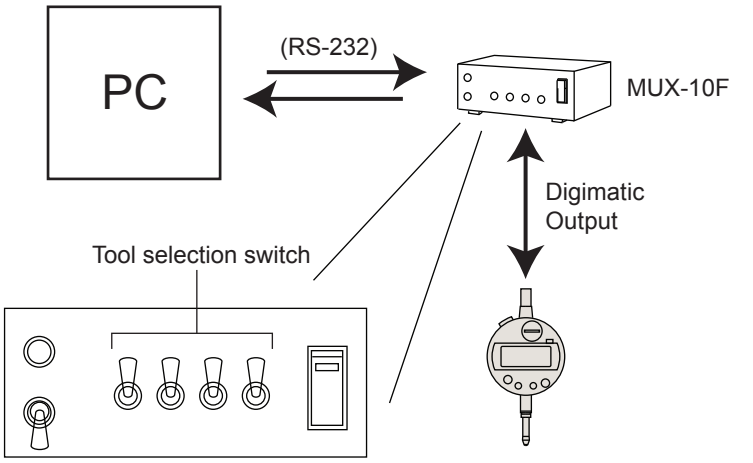

Commands (ASCII)	Transfer channels
1 (ASCII corde31) CR	1
2 (ASCII corde32) CR	2
3 (ASCII corde33) CR	3
4 (ASCII corde34) CR	4
A (ASCII corde41) CR	1, 2, 3, 4
B (ASCII corde42) CR	1, 2, 4
C (ASCII corde43) CR	1, 3, 4
D (ASCII corde44) CR	2, 3, 4
E (ASCII corde45) CR	1, 2, 3
F (ASCII corde46) CR	1, 2
G (ASCII corde47) CR	1, 3
H (ASCII corde48) CR	1, 4
I (ASCII corde49) CR	2, 3
J (ASCII corde50) CR	2, 4
K (ASCII corde51) CR	3, 4

Figure 3.17: (Left)Connection diagram of the digimatic gauge, the multiplexor and the computer; (Right) Command table (Mitutoyo Cat2)

3.6.4 LabVIEW Program

The data acquisition units are controlled by a program specifically designed for the ACAR experiment and it is written in LabView 7.0. In this project, we are interested in the counts and the displacement that the movable platform moves. Here are the features of the program:

3.6.4.1 Data Structure

1. An array for storing counts, in which the element numbers are specified by the resolution and the maximum readings of the digimatic measuring gauge. The array size equals to the maximum readings of the digimatic measuring gauge divided by the resolution (length of the small intervals from the measurement).

2. An integer type variable stores the counts of the previous cycle.

3.6.4.2 Procedures

1. Initialize the array storing the counts. (Default value in each elements are zero)

2. Initialize the RS-232 port for the communication with the digimatic measuring gauge.

3. Initialize the DAQmx card for the communication with the internal counter register.

4. Send a command [1 (ASCII code 31) CR]to the multiplexer requires the multiplexer to send the reading of the gauge back to the computer.

5. Wait for 0.2s to ensure the requesting signal has reached the multiplexer.

6. Retrieve the DISPLACEMENT from the communication port and read the COUNTS in the internal register of the counter through DAQmx.
7. Calculate the COUNTS increased (Subtracting the new COUNTS from the old counts.
8. Determine the index (Divide the DISPLACEMENT by the Max. DISPLACEMENT and multiply by the size of array and round it off to the nearest integer.)
9. Add the new counts to that array element.
10. Repeat the procedure (4)-(9) until the stop button is pressed.
11. Save the array into a text file.

3.6.4.3 Output

1. The measured value of the digimatic measuring gauge and the counts received are saved in a text file in csv format.
2. The counts array is saved to a text file if 1)The “Stop” button is pressed, or 2)The “Save” button is pressed.

3.7 Testing Materials

1. Aluminium (0.90mm x 21.2mm x 22.75mm) , (0.90mm x 22.6mm x 22.75mm)
2. Copper(3.75mm x 18.95mm x 16.80mm) , (3.75mm x 19.30mm x 17.10mm)
3. Stainless steel (0.90mm) x 2

Chapter 4

Result and Data Analysis

The experimental data gives the relation between the counts and the displacements. To make a better interpretation of the data, the counts will be divided by the total counts to normalize the graph. The displacement will be used to calculate the angular deviation from 180^o. The angular deviation θ are calculated in the following way:

$$\begin{aligned} \theta \approx \tan\theta &= \frac{\text{Displacement}}{\text{Gauge-Source distance}} \\ &= \frac{\text{Displacement}}{700mm} \end{aligned} \tag{4.1}$$

Then the treated data are plotted with $\frac{N(\theta)}{N}$ against θ. This angular deviation is expressed in radians while the normalized counts do not have a unit. The physical meaning of θ has been deducted in the previous section, which is equal to the p_z , the z component of momentum of the annihilated electrons in the units of mc[9]. The curves have been normalized such that the area under the graph gives unity. There exists some background counts at high angles which are random coincidences due to background radiation and the rays that penetrate the lead blocks. Similar to the work of DeBenedetti, the standard derivation which is calculated as the square root of the counting rate, shows only for the highest point[9].

The parabolic fit and Gaussian fit are also shown in the graph. To get θ_{max}, we consider the coefficients of the parabolic fit a,b,c. The parabolic equation reads $y = ax^2 + bx + c$. The x-intercept are the roots of the equation and equals:

$$x = \frac{-b \pm \sqrt{b^2 - 4ac}}{2a} \tag{4.2}$$

And the maximum angular derivation gives

$$\theta_{max} = \frac{|x_1| + |x_2|}{2}$$

The treated data are also plotted with $\frac{N(\theta)}{N}$ against θ^2. Which is followed by a linear fit.To get θ_{max}, we consider the coefficients of the parabolic fit a,b. The equation of straight line gives $y = ax + b$ and the x-intercept equals $\frac{-b}{a}$. Thus

$$\theta_{max} = \sqrt{\frac{-b}{a}} \tag{4.3}$$

The following constants are utililized in the calculation:

$$\begin{aligned} \hbar &= 1.0546 \times 10^{-34} Js \\ m &= 9.1094 \times 10^{-31} kg \\ e &= 1.602 \times 10^{-19} C \\ c &= 3 \times 10^{8} ms^{-1} \end{aligned}$$

4.1 Aluminium

4.1.1 ACAR Result

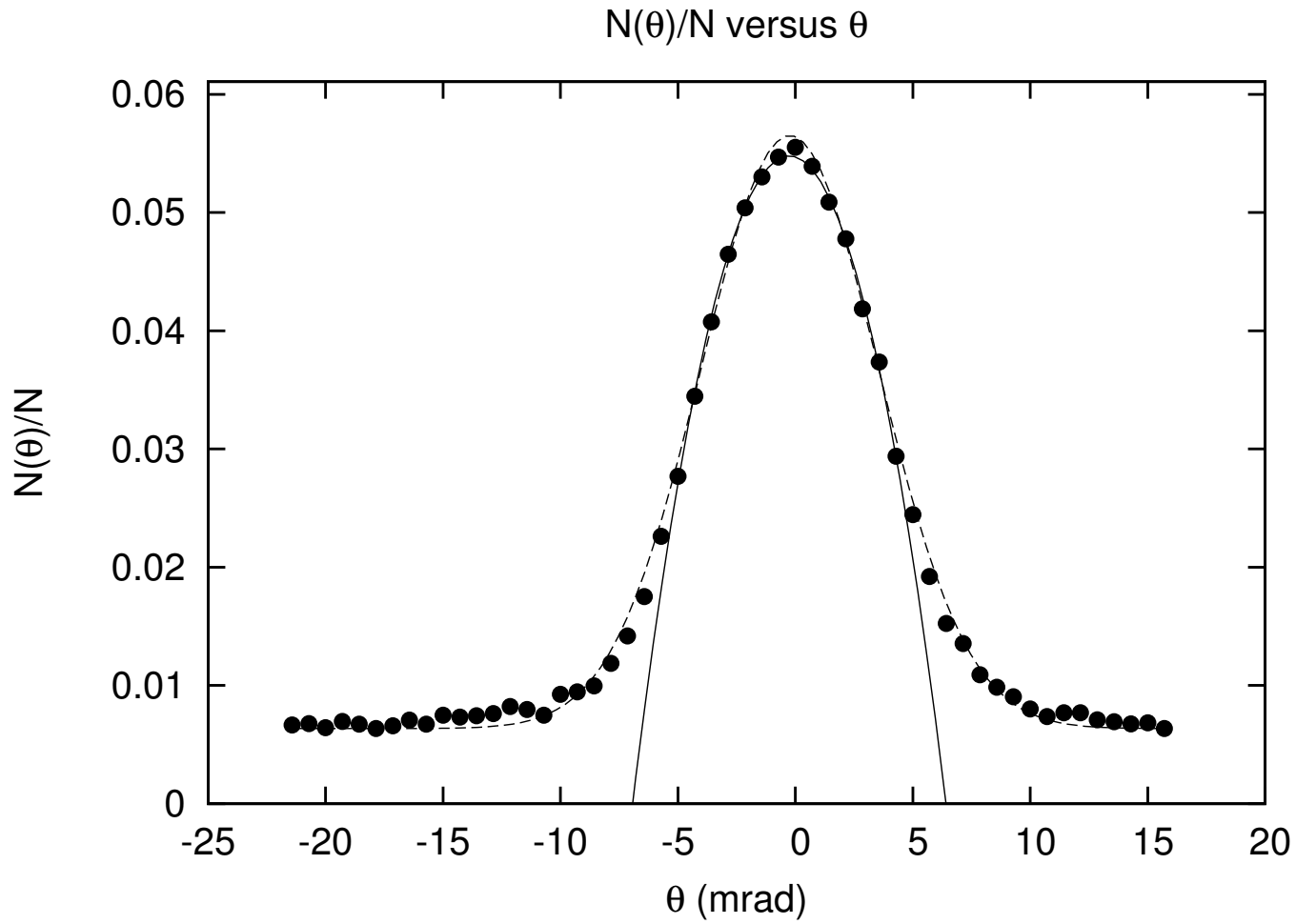

Figure 4.1: Angular Distribution from Al (A plot of $\frac{N(\theta)}{N}$ against θ)

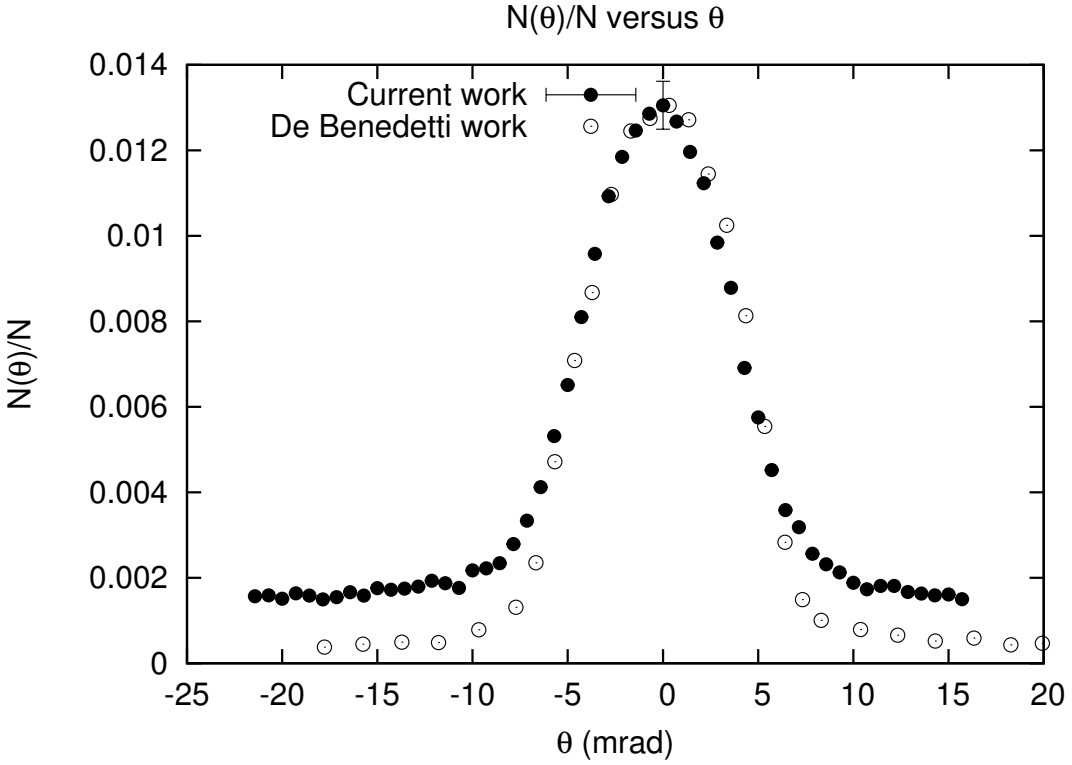

Figure 4.2: Comparison with DeBenedetti's work [9]

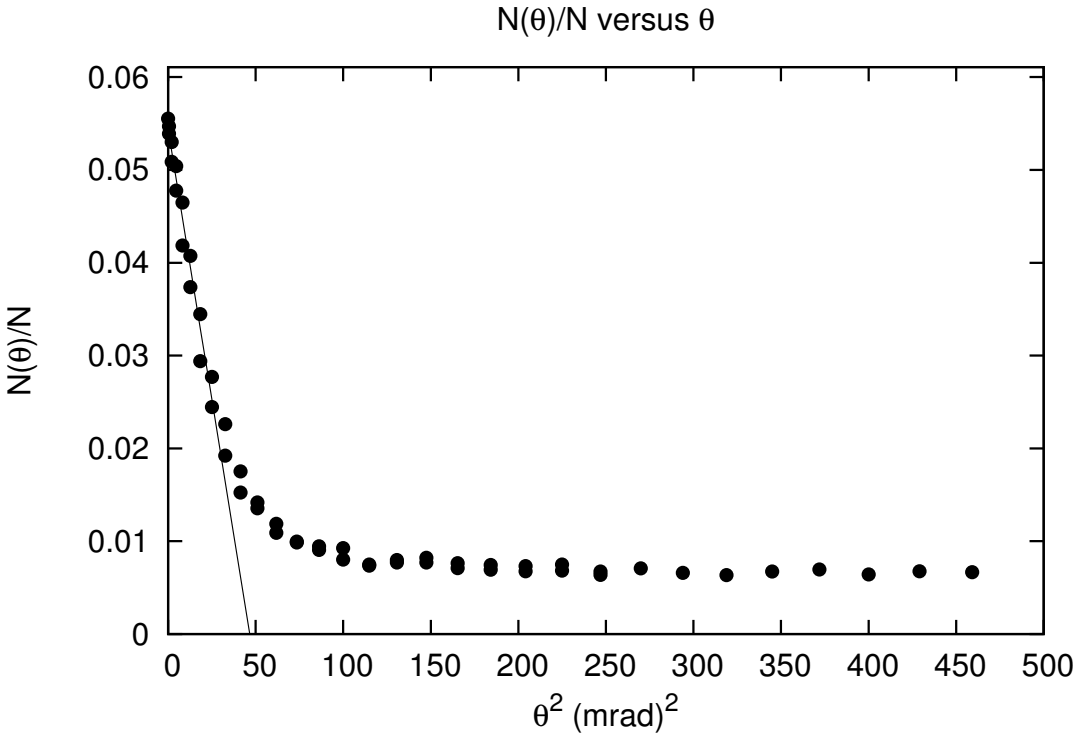

Figure 4.3: A plot of $\frac{N(\theta)}{N}$ against θ^2

4.1.2 Fermi-Energy Calculation

The maximum angular deviation θ_{max} in the parabolic plot is

$$\theta_{max} = \frac{6.413 + 6.930}{2} = 6.672 mrad \tag{4.4}$$

The maximum angular deviation θ_{max} in the linear plot is

$$\theta_{max} = \sqrt{0.0544081/0.00116694} = 6.83 mrad \tag{4.5}$$

The z-component of Fermi momentum is

$$p_z = 1.867 \times 10^{-24} \tag{4.6}$$

The Fermi momentum is

$$P_F = 1.867 \times 10^{-24} \tag{4.7}$$

The Fermi wave number is

$$k_F = \frac{p_F}{\hbar} = 1.770 \times 10^{10} m \tag{4.8}$$

The Fermi energy is

$$E_F = \frac{P_F^2}{2m} = 11.94 eV \tag{4.9}$$

4.1.3 Comparison with Fermi-gas model

	Fermi-gas model	Experimental value	Percentage difference
Maximum angular deviation θ_{max}	6.75mrad	6.83mrad	1.19%
Fermi momentumP_F	1.846×10^{-24}	1.867×10^{-24}	1.14%
Fermi wave numberk_F	1.750×10^{10}	1.770×10^{10}	1.14%
Fermi energyE_F	$12.324eV$	$11.94eV$	3.12%

4.2 Copper

4.2.1 ACAR Result

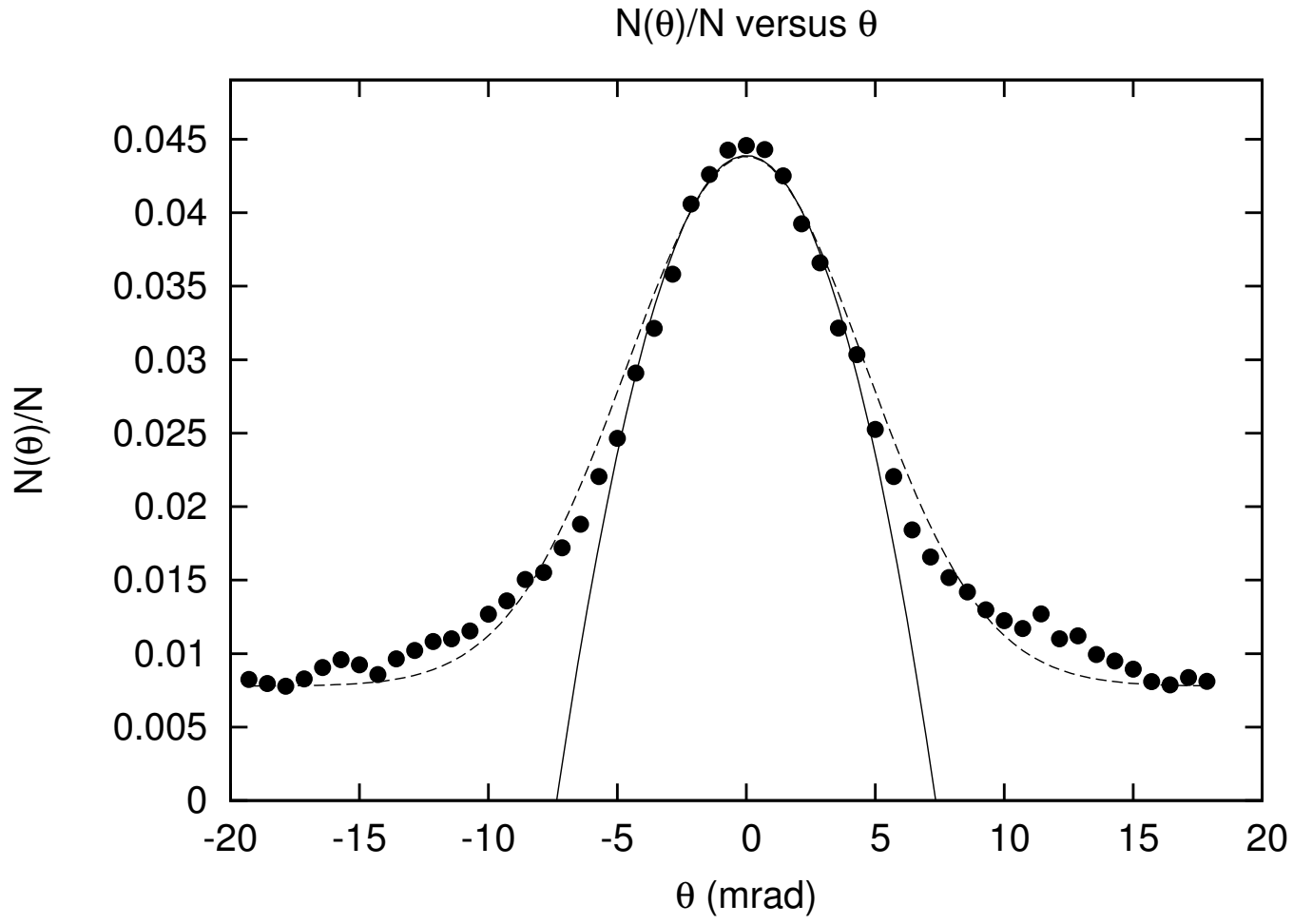

Figure 4.4: Angular Distribution from Cu (A plot of $\frac{N(\theta)}{N}$ against θ)

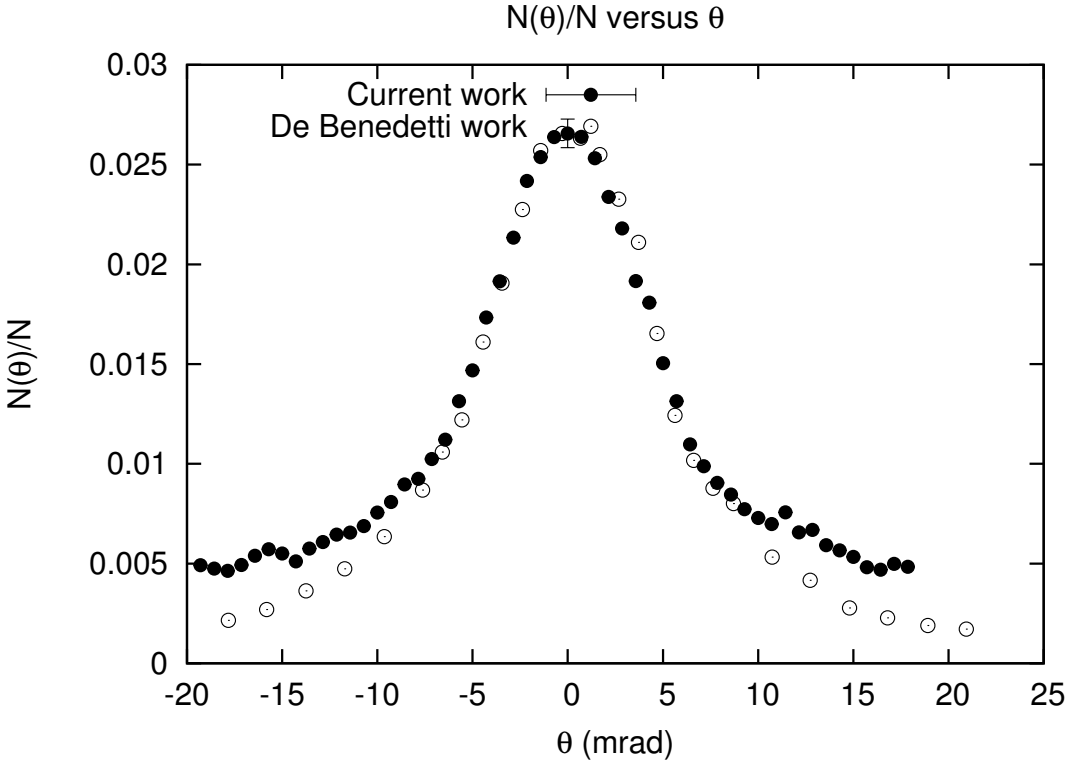

Figure 4.5: Comparison with DeBenedetti's work[9]

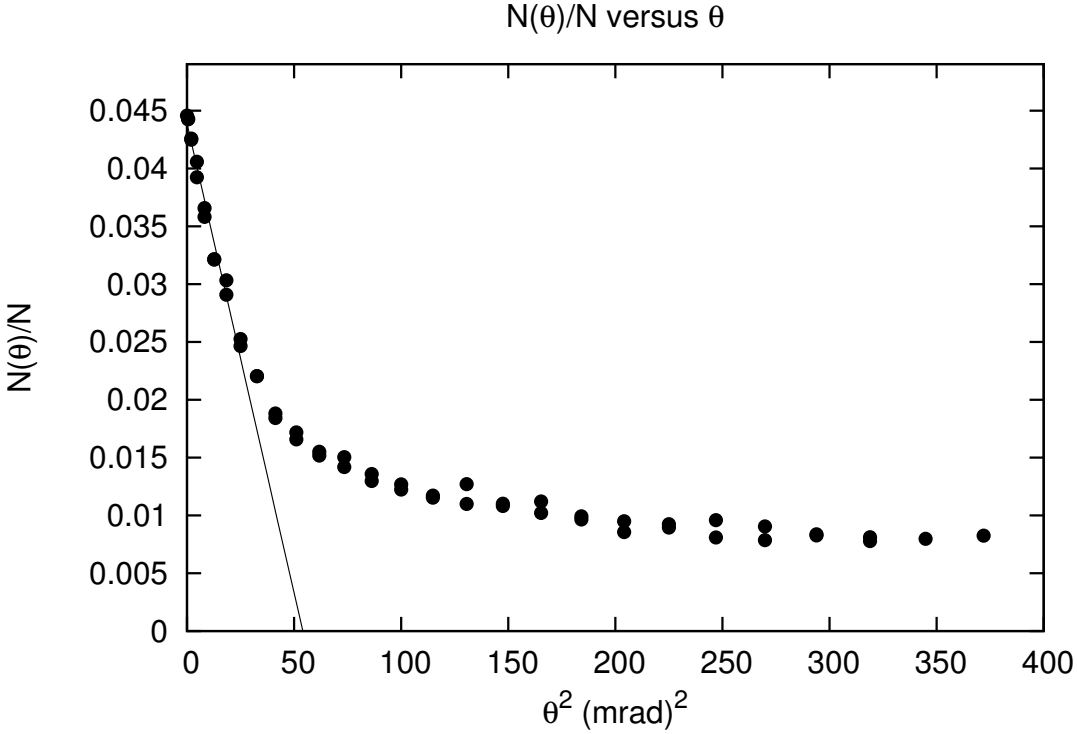

Figure 4.6: A plot of $\frac{N(\theta)}{N}$ against θ^2

The maximum angular deviation θ_{max} in the parabolic plot is

$$\theta_{max} = \frac{7.348 + 7.354}{2} = 7.351 mrad \tag{4.10}$$

The maximum angular deviation θ_{max} in the linear plot is

$$\theta_{max} = \sqrt{0.0438954/0.000811792} = 7.353 mrad \tag{4.11}$$

The z-component of Fermi momentum is

$$p_z = 2.0094 \times 10^{-24} \tag{4.12}$$

The Fermi momentum is

$$P_F = 2.0094 \times 10^{-24} \tag{4.13}$$

The Fermi wave number is

$$k_F = \frac{p_F}{\hbar} = 1.961 \times 10^{10} m \tag{4.14}$$

The Fermi energy is

$$E_F = \frac{P_F^2}{2m} = 13.835 eV \tag{4.15}$$

4.2.2 Comparison with Fermi-gas model

	Fermi-gas model	Experimental value	Percentage difference
Maximum angular deviation θ_{max}	5.23mrad	7.353mrad	1.19%
Fermi momentumP_F	1.429×10^{-24}	2.0094×10^{-24}	40.6%
Fermi wave numberk_F	1.356×10^{10}	1.961×10^{10}	44.6%
Fermi energyE_F	$7eV$	$13.835eV$	97.6%

4.3 Stainless Steel

4.3.1 ACAR Result

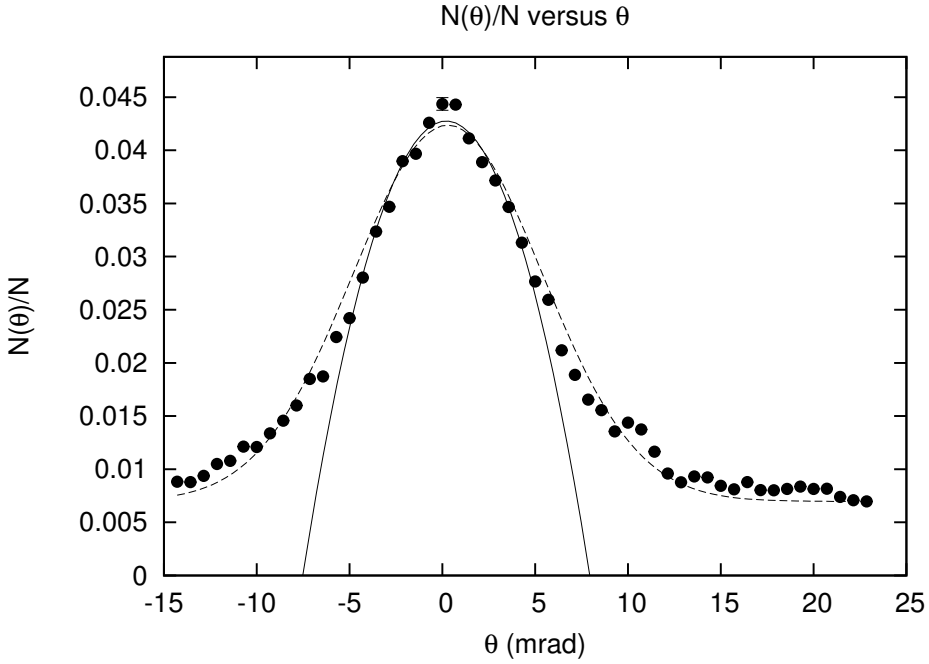

Figure 4.7: Angular Distribution from Fe (A plot of $\frac{N(\theta)}{N}$ against θ)

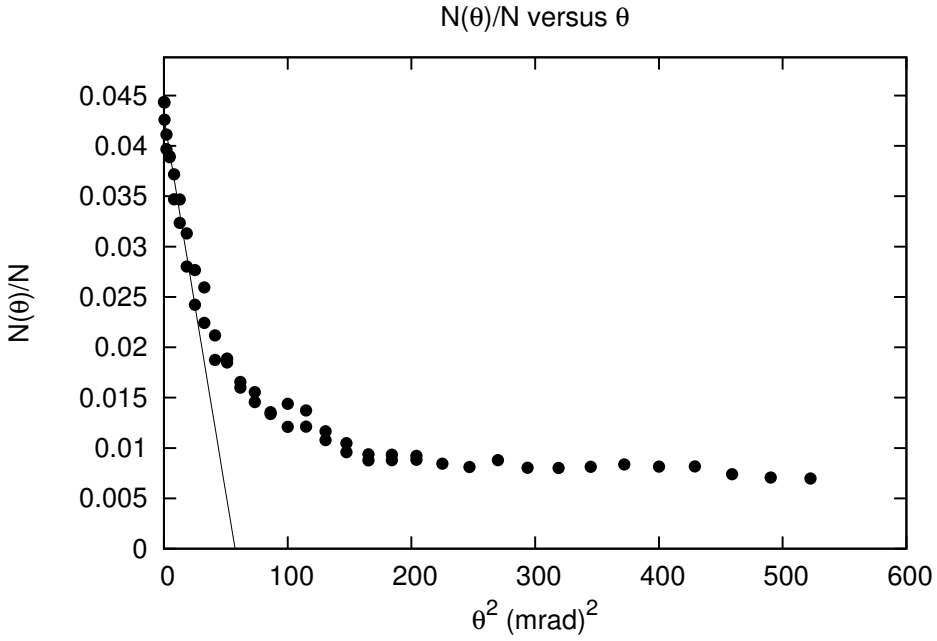

Figure 4.8: A plot of $\frac{N(\theta)}{N}$ against θ^2

4.3.2 Fermi-Energy Calculation

The maximum angular deviation θ_{max} in the parabolic plot is

$$\theta_{max} = \frac{7.943 + 7.5204}{2} = 7.732 mrad \tag{4.16}$$

The maximum angular deviation θ_{max} in the linear plot is

$$\theta_{max} = \sqrt{0.042874/0.000746015} = 7.581 mrad \tag{4.17}$$

The z-component of Fermi momentum is

$$p_z = 2.072 \times 10^{-24} \tag{4.18}$$

The Fermi momentum is

$$P_F = 2.072 \times 10^{-24} \tag{4.19}$$

The Fermi wave number is

$$k_F = \frac{p_F}{\hbar} = 1.965 \times 10^{10} m \tag{4.20}$$

The Fermi energy is

$$E_F = \frac{P_F^2}{2m} = 14.706 eV \tag{4.21}$$

4.3.3 Comparison with Fermi-gas model

	Fermi-gas model	Experimental value	Percentage difference
Maximum angular deviation θ_{max}	6.59mrad	7.581mrad	15%
Fermi momentumP_F	1.800×10^{-24}	2.072×10^{-24}	15.1%
Fermi wave numberk_F	1.707×10^{10}	1.965×10^{10}	15%%
Fermi energyE_F	$11.1eV$	$14.706eV$	32.4%

Chapter 5

Discussion

5.1 ACAR observation

The result for Aluminium is satisfactory and it works well with the Fermi Gas Model. However, the other two metals, Copper and Stainless steel, are failed to explain by the Fermi-Gas Model. DeBenedetti suggested that there are three types of metals that can be classified according to the ACAR results[8]. Group A elements, which consists of "Li, Na, Be, Mg, Al. Ge, Sn, and Bi" have distributions that ended at a sharp break and the distribution curve have an inverted parabola at the center and a long flat tail to large angle [8]. Group B metals are "Ca, Ba, Zn, Cd, and Pb" , they also have a central parabola but the tail is comparatively larger than group A[8]. The last group, group C, consists of "Cu, Ag, Au, Fe, Co, Ni, Rh, Pd, Pt and W" do not follow this distribution and show a "bell-shaped angular distribution"[8].

Group C are commonly known as the transitional metals and there are some properties in transition metals make them failed with the Fermi-gas model. The Group A are alkali or alkali earth metals that has a simpler electron structure . So the electron momentum distribution can be well explained by the Fermi-gas model.

5.2 Tuning the equipments

The ACAR experimental setup didn't come in handy or I should say , it didn't work at all. In scientific experimental research, it is of paramount importance that all the equipments are running properly and revealing physical explainable results.

5.2.1 This Year and Last Year

The ACAR experimental setup was to be reconfigured this year. Last year, the ACAR system consists of its basic electronic setup, a Linear Variable Differentiable Transformer (LVDT) and a PC data acquisition card. The use of LVDT is to get the displacement of the movable platform from the central line, which is similar to the digimatic measuring gauge. It consists of a primary coil, secondary coil and a magnetic core. The relation between the position of the core is linear to the change of voltage. Thus, reading the voltage will give the position of the core, i.e. the position of the movable platform.

Similar to this year's setup, the scintillation detectors generate pulses when the annihilation gamma ray is detected. The pulses are amplified, passed through a voltage-selection window and finally entered the coincidence unit. The coincidence unit generate a logic pulse if the two pulses occur at almost at the

same time. The practice of last year aimed to use the logic pulse to trigger the reading of LVDT through the PC data acquisition card.

This year, the digimatic measuring gauge is used to acquire the displacement of the movable platform from the central line. Thus a new technique is used to acquire the information and the program has to be rewritten. Also, Germanium-68 is used to replace Sodium-22, Germanium-68 has to be ordered and it takes several months to arrive.

5.2.2 Problems related to the Modular Electronics Instruments

It is very difficult to deal with electronics. They are expensive but will still fail in operation. Or they are hard to work with other electronics. A complete checking has been done to those modular electronics such that the experiment can be performed decently.

An oscilloscope is our friend, it reveals any improper signals generated from the instruments and we would determine if the instrument works properly by looking at the shape, amplitude and trigger time of the pulse. It should give a correct signal if it works properly.

High Voltage Supply It is hard to test with the high voltage supply but as long as the detector is working properly, the power supply would be all right. One high voltage supply has been replaced due to internal failure and gives out noises to the detector. And the replaced one has repaired one time due to failure in internal circuit. They are functioning decently till now.

Scintillation detector The scintillation detector should give a unipolar pulse which represents the surge of electrons generated in the photomultiplier. Both detectors have been tested with a liquid Na22 source, and the pulses come more frequently when the source is put nearby. The tube is also tested by connecting the detectors to a working DBS instruments and two characteristic pecks at 0.511Mev and 1.27 MeV for both tubes. The optimum voltage for both detectors are also found to make the detector function properly.

Preamplifier and Amplifier When the pulses passed through the preamplifier, they are stabilized and the pulse shape has been changed. The preamplifier gives a semi-Gaussian unipolar pulse with amplitude revealing the amount of gamma ray energies(Ortec). Both of the amplifier has been checked if the pulse generated is normal and have similar amplitude for most of the signal(Coincidence gamma ray)

Single Channel Analyzer The single channel analyzer equipped with timing module has two basic functions: Selecting pulses and Delay pulses. A series of checking has been made to find out the window setting on the SCA panel: The count rate is monitored by the counter, collect the number of counts(events) in a time interval, repeat counting with different windows setting. Then plot a graph of counts rate against the “windows setting”. A suitable window can be found by the “windows setting” that has a huge drop in counts rate. Actually, one SCA module set window with upper and lower limit while the other one set window with lower level and the window width.

For the former one, the “windows setting” would be either increasing the lower limit and fixing the upper limit maximum. A sudden decrease in counts rate will be observed. The lower and upper limit can be set such that the “great depression” bounded by the window.

For the latter one, the “windows setting” would be fixing the lower limit and decrease the windows size. A sudden decrease in counts rate will also be observed. The lower and window size can be set such that the “great depression“ has bounded.

The TSCA module also have the ability to delay the output signal. To get the correct delay setting, both of the TSCA outputs are connected to the oscilloscope (Channel 1 and channel 2). Set the triggering to one of the channel, the pulses from the other channel will flash with low frequency if the two signals are not in coincidence. Tune the delay setting and the pulses from the other channel will flash frequently but located far away. Tune the delay setting until both two pulses appear in the middle.

One of the TSCA module has been replaced.

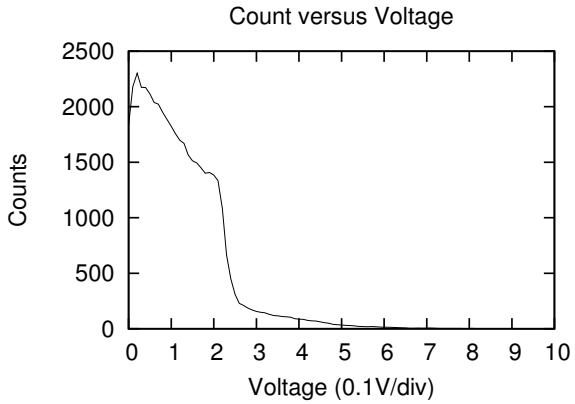

(a) Lower limit increase from 0V to 10V, fixed upper limit at 10V

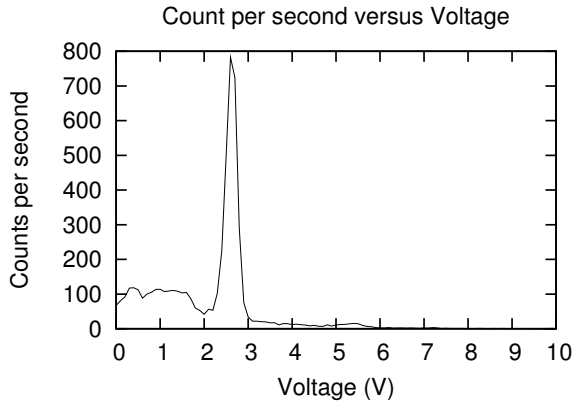

(b) Lower limit form 0V to 10V with a fixed window of 0.1V

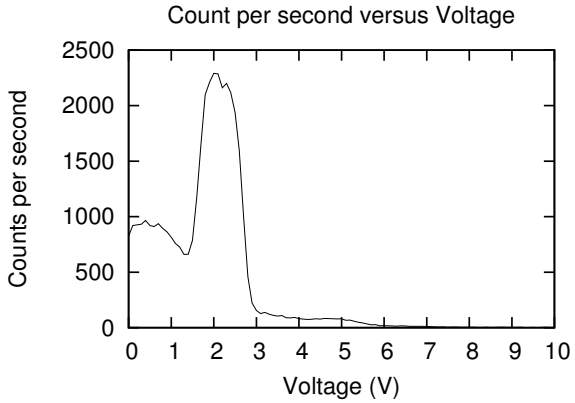

(c) Lower limit form 0V to 10V with a fixed window of 1V

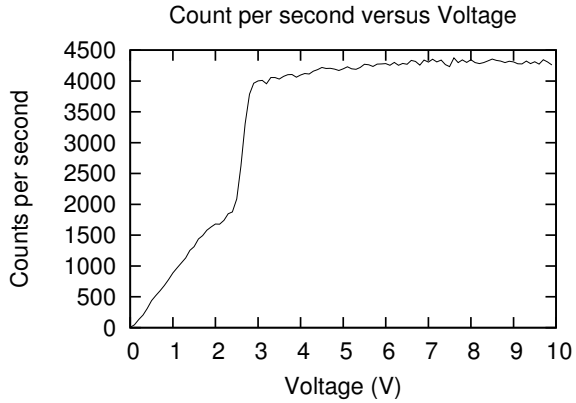

(d) Lower limit fixed at 0V . Window switch from 0V to 10V

Figure 5.1: TSCA test result

Coincidence Unit The coincidence unit can now read the coincidence pulses. To test this devices, the output of this unit will be connected to a counter. No counts should be detected if we have removed the sources.

5.2.3 Problems related to the ACAR Setup

The setup include the motor, the platforms and the sources. The motor has an automatic controlling unit and this simple unit can control the movement of the platform. The platform "swinging" about the central axis periodically and it works perfectly. A set of motor gear is removed so that the platform can swing faster.

The sources Germanium-68 finally arrived at February 2010. Before the arrival of the Germanium-68, Sodium-22 is used to test the apparatus and the experiment cannot start until the arrival of the isotope source. The Ge-68 has an extremely small physical size so it can be sandwiched inside the samples like cream crackers. The samples were made with the help of technician and the size is similar to the source. The problem arrives when the lead blocks setup designed for this experiment have disappeared and only a small fraction has been found. A new lead "building" has been built using several lead blocks such that the radiation can only leaves through the two opposite gauges.

When the cracker-like sandwiched sample was put inside the lead "building" and another problem arised. The "cream crackers" has to be placed at the intersection of two lines in the space. The first line is the perpendicular line growing from the center of the central axis and have equal distance with the two detectors (The vertical lines at the center). The second line is the line joining the center of the scintillating crystal (Or the center of the circular surface of the scintillator). To align the sample properly, we could utilize a string joining the detectors to visualize the latter line and put the sample at the intersection. As the procedure has to be done every time the sample is changed, the lead block has been marked with the suitable position.

5.2.4 Problems related to the Data Acquisition Units

The Data Acquisition Units work with the computer to acquire data from the setup. This tuning part has spent 90% of the project time.

The Digimatic measuring gauge and multiplexor The digimatic measuring gauge incorporates with the multiplexor to return the readings to computer. The purpose of the multiplexor is to communicate between the gauge and the computer. However, the multiplexor has never been working since it purchased. A series of investigation has made to make the multiplexor working. A RS-232 cable has made by technician such that it can communicate with the computer. However, the cable cannot be any type but a straight-through RS-232 cable.

The terminal software in the computer helps the testing of the devices. By monitoring the COM part in the computer, the input and output are shown. Commands can be typed in and results are returned if all the settings of COM port are correct. The COM port setting has several parameters, some of them are fixed by the multiplexor and the computer settings have to follow it. Some of them are variable, such as the baud rate, it can be tuned at the panel and changed at the computer settings. Once the settings are finished and the devices are connected, the commands can be typed to observe any output from the

multiplexor.

A sample LabVIEW program has been downloaded and modified for testing. Modification includes changing the COM port setting, changing the frequency for acquiring data and grubbing usable information from the returned ASCII codes. However, this device cannot support instance data acquisition. The time interval between sending a command and retrieving information spends about 0.2s and this time cannot go smaller. Thus, we have a different data acquisition algorithm than last year.

Multifunction Data Acquisition (DAQ) Card and Connection board The DAQ card is the same as last year but the connection board has been replaced. The counter function in the card is utilized in the ACAR experiment. The new connection board contains pinholes and different from the interface of coaxial cables. An adapter is made to connect the coaxial head with two wires, the two wires are connected to the connection board with pins. Later, another adapter is made to connect the coaxial head into a pin directly to reduce the noise.

The DAQ counter function is not working properly as there are sudden purges of counts that ruin the data. Many efforts are made to get the counter working. The testing tools are the signal or pulse generator and the coincidence pulse from the scintillators. At first, the signal generator was used to generate regular square pulse for the counter, the counters counts well with it. Some unknown operation causes the counter to stop working and it didin't read any signal. Later, it was discovered that the first adapter is broken and it was replaced, but the counter still didn't work.

In the period when the counter stop functioning, several approaches were tried to mimic the counter function. The analog voltage input in the DAQ card was utilized and the voltage value were input to computer. Like an oscilloscope, the new method reads the input voltage and trigger when there was sudden change in voltage. However, the maximum input rate is much lower than the concerned pulses. The analog input can do 10,000 sampling in a second without problem but it started generate problem when higher sampling rate is tested. Our concerned signals have a width of $1\mu s$ which requires at least 100,000Hz sampling to detect the change in voltage or we may lose most of the pulses. Thus, it is not a practical way to detect the pulse in the software, but a lot of time has been spent on discovering new methods and there were several successful methods for low frequency counting.

The counter resumed working and a pulse generator was used to test the device. The pulse generator generates pulses with similar pulse width as the coincidence pulse. The frequency of the pulse can be altered such that a lower frequency can be used (The coincidence pulse doesn't come very often). The pulse generator output pulses to the DAQ card and a modular counter at the same time. The counts taken by the card and the modular counter were compared and results shown that they are equal. The counter function were proved to be usable and reliable.

The DAQ card was connected with coincidence pulse of Germanium-68 for further test. A LabVIEW program was written for counting at a period of time repeatedly. Results shown that the the count rate is constant for most of the period but at some time, the count rate grew enormously. Generation of noise was suspected to create the counts. A new adapter was made and reduce the some noise but with little help. Later it was discovered that the motor will generate E-M field that drives the electrons and trigger the counter, the noises are detected in oscilloscope as some small ripples in the screen. The small ripples have amplitude high enough to trigger the counter (The counter reads TTL signal).

Later, a metal box was used to shield the connection boards and a battery box was connected to the coaxial cables to reduce the noise by providing a negative voltage. With the help of the metal box and the battery, the noise problem has been solved and the whole setup can finally reading data properly.

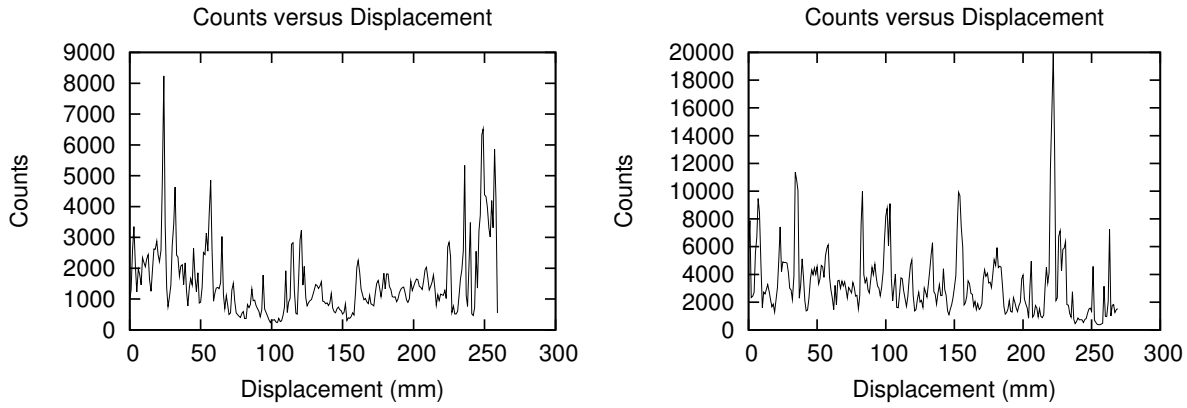

Figure 5.2: Results with noise, no angular distribution shown

5.3 Programing

Several programs have been written to complete this project. They are for data acquisition and data analysis.

5.3.1 LabVIEW Programs

LabVIEW has been used widely in this project. Several programs were written in LabVIEW for acquiring data and testing the devices. The first program made is the one for controlling the multiplexor. This program was a sample program downloaded from the official website. The block diagrams were understood by Internet research. The basic technique were learned within several weeks through self-learning and finally a workable but not elegant program was born. This program has proved the multiplexor is working properly. Several programs were also written for testing and they have been mentioned in the previous section.

The last or the most important program made is the one which are collecting the information from the data acquisition units. This program was developed after the arrival of the source. It has incorporated the basic function of controlling the multiplexor, the reading of counts from the DAQ counter as well as a new data treatment algorithm. It was developed to automate the data acquisition so the program runs continuously until the user ends it. This program writes the raw data to a file continuously and can save the ACAR result during the running of the program. And it directly shows the ACAR plot in the screen.

5.3.2 C++ Programs

C++ is a programing language that is very handy in coding. Several programs were written in C++ for data analysis. Basically, they read the ACAR result, treat the data and output the data for graph plotting and curve fitting using GNU Plot.

5.3.3 GNU Plot

GNU Plot is a handy tool for professional graph making. It can generate high quality graph in pdf format. The plotting script was output by C++ program and leads the GNU Plot to read several files. Each files contains a set of data for 1) Plotting Points with or without error bars, 2) Parabolic fitting 3)Gaussian Fitting.

5.4 Improvement

5.4.1 Extending the range of motor

As we shall see, the angular distribution of some metals are very wide. The motor is confined within a small region. Thus the movable platform cannot move too far away from the central axis. The motor has to be extent such that the scintillator can scan through a larger angle.

5.4.2 Stronger Positron Source

To increase the resolution, the width of the narrow opening of the two lead blocks has to be decreased. The decrease in the width decrease the number of gamma ray entering the scintillation detectors. The count rate is about 10 counts per second in the central axis if the width is 2mm. However, the resolution of the present setup is 2mrad. For a better result, the resolution has to go down 0.5mrad which leads to a 16 times smaller count rate. Thus if the count rate has to be maintained or increased, a stronger source is required.
A stronger positron source has the following benefit:

1. The time for one ACAR experiment can be lessen as the counts accumulated increase very quickly.
2. The width of the opening can be decreased to have a better resolution

But the price of a stronger positron source is very high and it increases the danger of handling the radioactive material.

5.4.3 Better Remote control

The LabVIEW can be remotely controlled by remote desktop. However, the performance of remote desktop is poor and the data update is slow. A better function is found in the LabVIEW package that the running LabVIEW can be accessed through web server. A computer installed with LabVIEW running library can access the web page and monitor the labVIEW program. The front panel is pre-downloaded from the server and only a small amount of data is required to be transferred for updating. This is a better choice than running a remote desktop. However, some technique problem has to be solved before the on-line program can be controlled. The motor is not controlled in LabVIEW, so it is the choice for the future user to add the control function of the motor.

Chapter 6

Conclusion

The electron momentum distribution of Aluminium can be well explained by the Fermi gas model. The Fermi-energy and Fermi-momentum found in the experiment is $1.867 \times 10^{-24} Ns$ and $11.94 eV$ respectively. The results has a 3.12% and 1.14% deviation from the theoretical value of Fermi Gas model respectively. On the other hand, the copper and stainless steel, in which the experimental values have large deviations from the theoretical values, are failed to be explained by the Fermi Gas Model. Graphical plotting of the angular distribution has shown that there is a shape break at certain angle in the Aluminium angular distribution. However, the curve is broad and wide for the copper and stainless steel, which do not show a shape break at any point. Thus, a parabolic fitting cannot be applied to these two metals. The physical reasons are worth to investigate.

Bibliography

[1] Michael Charlton and John Walkin Humberson. Positron physics. 2000.

[2] Chung-choi. Cheng. Positron beam studies of fluorine implanted gallium nitride and aluminium gallium nitride [electronic resource] / by cheng chung choi. Master's thesis, University of Hong Kong, 2010.

[3] Bernd Crasemann, D. E. Rehfuss, and H. T. Easterday. Disintegration of *ge*68. *Phys. Rev.*, 102(5):1344–1346, Jun 1956.

[4] Enrico Fermi. *Positron solid state physics : proceedings of the International school of physics "Enrico Fermi", Varenna on Lake Como, Villa Monastero, 14-24 July 1981 : course LXXXIII*. North-Holland [for the Italian physical society], Bologna; Amsterdam; New York, 1983.

[5] Enrico Fermi. *Positron spectroscopy of solids*. IOS Press ; Distributor in Japan, Ohmsha, Amsterdam; Washington, DC; Tokyo, Japan, 1995.

[6] Glenn F. Knoll. *Radiation detection and measurement / Glenn F. Knoll.* Wiley, New York, 2000.

[7] R. Krause-Rehberg and H. S. Leipner. *Positron annihilation in semiconductors : defect studies*. Springer, Berlin; New York, 1999.

[8] G. Lang and DeBenedetti. Angular correlation of annihilation radiation in various substances. *Phys. Rev.*, 108(4):914–921, Nov 1957.

[9] G. Lang, S. DeBenedetti, and R. Smoluchowski. Measurement of electron momentum by positron annihilation. *Phys. Rev.*, 99(2):596–598, Jul 1955.

[10] ORTEC. Ortec catalog, 2010.

[11] Eckert & Ziegler Isotope Products. Eckert & ziegler reference & calibration sources, 2008.

[12] Miles N. Wernick and John N. Aarsvold. *Emission tomography : the fundamentals of PET and SPECT*. Elsevier Academic Press, Amsterdam; Boston, 2004.

List of Figures

1.1 Schematic diagram of various positron research [2] . . . 3

2.1 Feynman Diagram showing e^+e^- Annihilation with the emission of 2 gamma rays (Left); Feynman Diagram showing e^+e^- Annihilation with the emission of 3 gamma rays (Right) [1]. . . . 6
2.2 Diagram of electron-positron annihilation, producing two 511 keV photons leaving in opposite directions. . . . 6
2.3 Decay Scheme for ^{68}Ge [3] . . . 7
2.4 2γ annihilation (Up) In the center-of-mass frame (Down) In the laboratory frame [5] . . 9

3.1 Schematic Diagram for the ACAR spectrometer . . . 13
3.2 Schematic diagram for the 1D ACAR spectrometer and the critical geometrical parameters 13
3.3 Left: Ge-68 POSK Configuration[11]; Right: Sources and Sample . . . 14
3.4 The photoelectric effect(WILKINSON) . . . 15
3.5 The Compton scattering(WILKINSON) . . . 16
3.6 The Pair Production(WILKINSON) . . . 16
3.7 Three interaction mechanisms for different energy gamma-ray(WILKINSON) . . . 17
3.8 Schematic Diagram for electronics connection . . . 18
3.9 Signal coming out from the Scintillation Preamplifier(2V, 50μs) . . . 19
3.10 Signal coming out from the Amplifier (2V, 5μs) . . . 19
3.11 Signal selection through Single-Channel Analyzer[10] . . . 20
3.12 Signal coming out from the Single-Channel Analyzer (2V, 250ns) . . . 20
3.13 Coincident requirement[10] . . . 20
3.14 I/O Connector diagram for 16-Channel E Series DAQ device . . . 21
3.15 Connection diagram of the coaxial cable and the DAQ device . . . 21
3.16 Digimatic Measuring Gauge (1"/25.4mm range model)(Mitutoyo Cat) . . . 22
3.17 (Left)Connection diagram of the digimatic gauge, the multiplexor and the computer; (Right) Command table (Mitutoyo Cat2) . . . 23

4.1 Angular Distribution from Al (A plot of $\frac{N(\theta)}{N}$ against θ) . . . 26
4.2 Comparison with DeBenedetti's work [9] . . . 27
4.3 A plot of $\frac{N(\theta)}{N}$ against θ^2 . . . 27
4.4 Angular Distribution from Cu (A plot of $\frac{N(\theta)}{N}$ against θ) . . . 29
4.5 Comparison with DeBenedetti's work[9] . . . 30
4.6 A plot of $\frac{N(\theta)}{N}$ against θ^2 . . . 30

4.7 Angular Distribution from Fe (A plot of $\frac{N(\theta)}{N}$ against θ) 32
4.8 A plot of $\frac{N(\theta)}{N}$ against θ^2 32

5.1 TSCA test result 36
5.2 Results with noise, no angular distribution shown 39

A.1 The Front Panel of the LabVIEW program 45
A.2 The Block diagram of the LabVIEW program 46
A.3 Web remote control features of the LabVIEW program 47

Appendix A

Data Acquisition Program

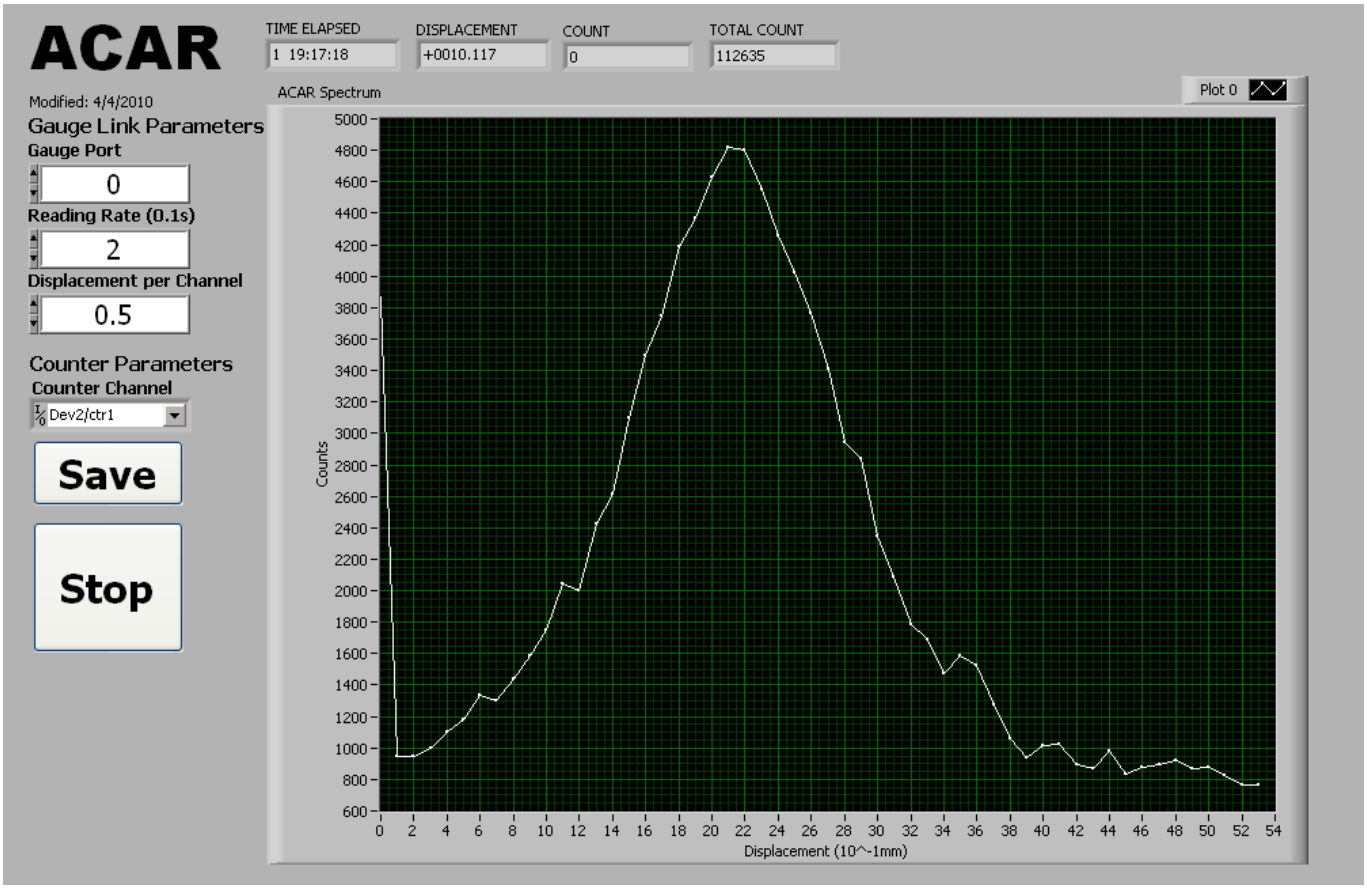

Figure A.1: The Front Panel of the LabVIEW program

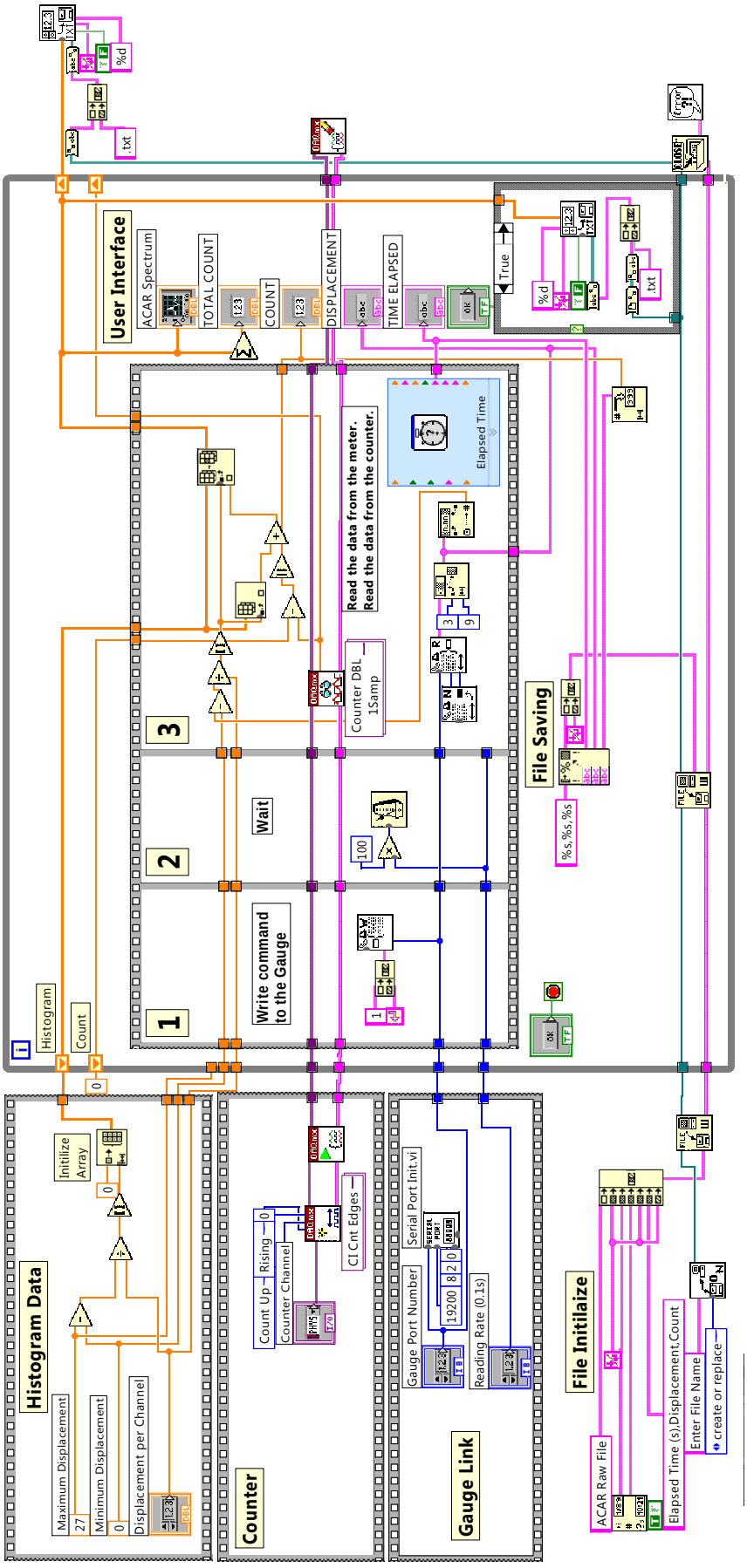

Figure A.2: The Block diagram of the LabVIEW program

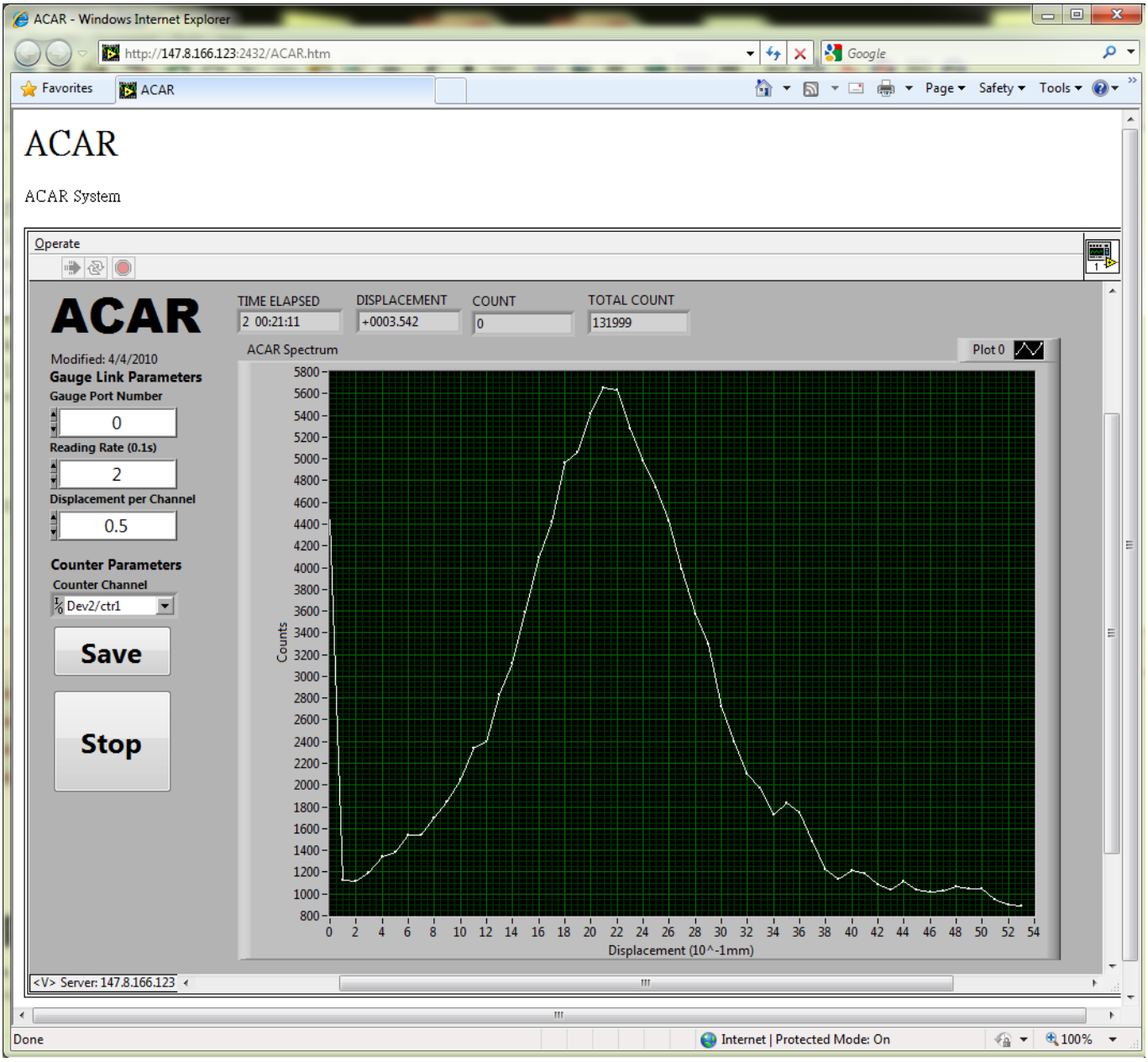

Figure A.3: Web remote control features of the LabVIEW program

Appendix B

Data Analysis Program and Scripts

Algorithm B.1 A C++ program for plotting graph

```
/*
Physics Project : ACAR
Name: Leung Wai Yan
UID: 2007132498
Date: 28/4/2010
This Program real a ACAR result file and plot in GNUPlot
Usage: ./acar <file name> <number of data> <number of data for parabolic fit>
*/
#include <stdlib.h>
#include <iostream>
#include <math.h>
#include <string>
#include <fstream>
using namespace std;
int peak (int* value, int size){
        int i;
        int maxvalue = value[1];
        int max = 0;
        for ( i = 1; i < size; ++i ){
                if (maxvalue < value[i]){
                        maxvalue = value[i];
                        max = i;
                }
        }
return max;
}
int min (int* value, int size){
        int i;
        int minvalue = value[1];
        int min = 1;
        for ( i = 1; i < size; ++i ){
```

```
                if (minvalue > value[i]){
                minvalue = value[i];
                min = i;
                }
        }
return min;
}

int main(int argc, char** argv)
{
int x[500];
int y[500];
int maxdata = atoi(argv[2]);
int width = atoi(argv[3]);
int i,low,high,background;
double sum;

// Initilize the array
for( i = 0 ; i < 500; ++i){
        y[i] = 0;
        x[i] = i;
}

// Initilize file I/O
ifstream infile;
infile.open(argv[1]);
if(infile.fail())
        return 0;

// Read the points from the file
i = 0;
while(infile >> y[i])
        i++;
infile.close();
// Get the sum of the counts
for( i = 1 ; i < 500; ++i){
        sum = sum+ y[i];
}

low = peak(y, maxdata) - width;
high = peak(y, maxdata) + width;
background = min(y, maxdata);
ofstream outfile;

// Output the drawing data
outfile.open("temp_plot1");
for( i = 1 ; i < maxdata; ++i)
```

```
        outfile << x[i] << "\t" << y[i]<<endl;
outfile.close();

// Output the drawing data for parametric fit
outfile.open("temp_plot2");
for( i = low ; i < high; ++i)
        outfile << x[i] << "\t" << y[i]<<endl;
outfile.close();

// Output the drawing data for gaussian fit
outfile.open("temp_plot3");
for( i = 1 ; i < maxdata; ++i)
        outfile << x[i] << "\t" << y[i] - y[background] <<endl;
outfile.close();

// Output the drawing script
outfile.open("temp_plot.s");
outfile << "g(x)=A1*exp( -((x-x1)/sig1)**2 )" <<endl;
outfile << "h(x)=g(x)+"<< y[background] <<endl;
outfile << "fit f(x) 'temp_plot2' via a,b,c" <<endl;
outfile << "fit g(x) 'temp_plot3' via A1,x1,sig1" <<endl;
outfile << "set yrange [0" << ":" << y[high-width] * 1.1<< "]" <<endl;
outfile << "set clip one" <<endl;
outfile << "set key left top" <<endl;
outfile << "set title \"Counts versus Displacement\"" <<endl;
outfile << "set ylabel \"Counts\"" <<endl;
outfile << "set xlabel \"Displacement\"" <<endl;
outfile << "set style line 1 lt 1" <<endl;
outfile << "set style line 2 lt 2" <<endl;
outfile << "set style line 3 lt 1 pt 7" <<endl;
outfile << "set term x11" <<endl;
outfile << "plot f(x) notitle with lines linestyle 1,\\" <<endl;
outfile << " 'temp_plot1' notitle with points linestyle 3,\\" <<endl;
outfile << " g(x) notitle with lines linestyle 2" <<endl;
outfile << "set term postscript eps enhanced level1" <<endl;
outfile << "set output '" << argv[1] << ".pdf" << "'" <<endl;
outfile << "replot" <<endl;
outfile << "set term x11" <<endl;
outfile.close();
system("gnuplot temp_plot.s");
return 0;
}
```

Algorithm B.2 A C++ program for plotting the $N(\theta)/N$ versus θ

```
/*
Physics Project : ACAR
Name: Leung Wai Yan
UID: 2007132498
Date: 28/4/2010
This Program real a ACAR result file and plot in GNUPlot
Usage: ./acar <file name> <number of data> <number of data for parabolic fit>
*/

#include <stdlib.h>
#include <iostream>
#include <math.h>
#include <string>
#include <fstream>
using namespace std;

int peak (double* value, int size){
        int i;
        double maxvalue = value[1];
        int max = 0;
        for ( i = 1; i < size; ++i ){
                if (maxvalue < value[i]){
                        maxvalue = value[i];
                        max = i;
                }
        }
        return max;
}
int min (double* value, int size){
        int i;
        double minvalue = value[1];
        int min = 1;
                for ( i = 1; i < size; ++i ){
                        if (minvalue > value[i]){
                                minvalue = value[i];
                                min = i;
                }
        }
        return min;
}
```

```
int main(int argc, char** argv){
double x[500];
double y[500];
```

```
int maxdata;
int width = atoi(argv[2]);
int i,low,high,background,mid;
double sum,xscale,error;
double r = 700.0; //70cm

// Initilize the array
        for( i = 0 ; i < 500; ++i){
        y[i] = 0;
        x[i] = i;
}

// Initilize file I/O
ifstream infile;
infile.open(argv[1]);
if(infile.fail())
        return 0;

// Read the points from the file
i = 0;
while(infile >> y[i])
        i++;
infile.close();
maxdata = i;
sum = 0;

// Get the sum of the counts
for( i = 1 ; i < 500; ++i){
        sum = sum+ y[i];
}

mid = peak(y, maxdata);
low = mid - width;
high = mid + width;
background = min(y, maxdata);
error = sqrt(y[peak(y, maxdata)])/sum;

// Get the x-scaling factoe
xscale = (27.0 / maxdata) /r * 1000;
ofstream outfile;

// Output the drawing data
outfile.open("temp_plot1");
for( i = 1 ; i < maxdata; ++i){
        if (i == mid)
                outfile << (x[i] - mid) * xscale << "\t" << y[i] / sum << "\t"
        else
```

```
                outfile << (x[i] - mid) * xscale << "\t" << y[i] / sum << "\t"
}
outfile.close();

// Output the drawing data for parametric fit
outfile.open("temp_plot2");
for( i = low ; i < high; ++i)
        outfile << (x[i] - mid) * xscale << "\t" << y[i] / sum << endl;
outfile.close();

// Output the drawing data for gaussian fit
outfile.open("temp_plot3");
        for( i = 1 ; i < maxdata; ++i)
outfile << (x[i] - mid) << "\t" << y[i] - y[background]*0.9<<endl;
outfile.close();

// Output the drawing script
outfile.open("temp_plot.s");
outfile << "f(x)=a*x*x+b*x+c" <<endl;
outfile << "g(x)=A1*exp( -((x-x1)/sig1)**2 )" <<endl;
outfile << "h(x)=g(x)/" << sum << "+"<< y[background] / sum <<endl;
outfile << "fit f(x) 'temp_plot2' via a,b,c" <<endl;
outfile << "fit g(x) 'temp_plot3' via A1,x1,sig1" <<endl;
outfile << "set yrange [0" << ":" << y[high-width] / sum * 1.1<< "]" <<endl;
outfile << "set clip one" <<endl;
outfile << "set size 0.7,0.7" <<endl;
outfile << "set key left top" <<endl;
outfile << "set title \"N({/Symbol q})/N versus {/Symbol q}\"" <<endl;
outfile << "set ylabel \"N({/Symbol q})/N\"" <<endl;
outfile << "set xlabel \"{/Symbol q} (mrad)\"" <<endl;
outfile << "set style line 1 lt 1" <<endl;
outfile << "set style line 2 lt 2" <<endl;
outfile << "set style line 3 lt 1 pt 7" <<endl;
outfile << "set term x11" <<endl;
outfile << "plot f(x) notitle with lines linestyle 1,\\" <<endl;
outfile << " 'temp_plot1' using 1:2:3 notitle with yerrorbars linestyle 3,\\"
outfile << " h(x/" << xscale << ") notitle with lines linestyle 2" <<endl;
outfile << "set term postscript eps enhanced level1" <<endl;
outfile << "set output '" << argv[1] << ".pdf" << "'" <<endl;
outfile << "replot" <<endl;
outfile << "set term x11" <<endl;
outfile.close();
system("gnuplot temp_plot.s");
return 0;
}
```

Algorithm B.3 GNU Plot scripts

```
#Declare functions
f(x)=a*x*x+b*x+c
g(x)=A1*exp( -((x-x1)/sig1)**2 )
h(x)=g(x)/23411+0.0028619
#Fit the data with our function
fit f(x) 'temp_plot2' via a,b,c
fit g(x) 'temp_plot3' via A1,x1,sig1
#Set pringing parameter
set yrange [0:0.108116]
set clip one
set size 0.7,0.7
set key left top
#The title and the axis
set title "N({/Symbol q})/N versus {/Symbol q}"
set ylabel "N({/Symbol q})/N"
set xlabel "{/Symbol q} (mrad)"
set style line 1 lt 1
set style line 2 lt 2
set style line 3 lt 1 pt 7
set term x11
# plotting command
plot f(x) notitle with lines linestyle 1,\
'temp_plot1' notitle with points linestyle 3,\
h(x) notitle with lines linestyle 2
set term postscript eps enhanced level1
set output './Data/Al_DeBenedetti.txt.pdf'
replot
set term x11
```

Appendix C

GNU Plot fitting logs

Algorithm C.1 Parabolic plot fitting logs for Aluminium

```
FIT: data read from 'temp_plot2'
#datapoints = 14
residuals are weighted equally (unit weight)
function used for fitting: f(x)
fitted parameters initialized with current variable values
Iteration 0
WSSR : 1907.54 delta(WSSR)/WSSR : 0
delta(WSSR) : 0 limit for stopping : 1e-05
lambda : 6.79856
initial set of free parameter values
a = 1
b = 1
c = 1
After 5 iterations the fit converged.
final sum of squares of residuals : 3.09471e-06
rel. change during last iteration : -1.70243e-13
degrees of freedom (FIT_NDF) : 11
rms of residuals (FIT_STDFIT) = sqrt(WSSR/ndf) : 0.000530413
variance of residuals (reduced chisquare) = WSSR/ndf : 2.81338e-07
Final set of parameters Asymptotic Standard Error
======================= ==========================
a = -0.00123152 +/- 1.927e-05 (1.564%)
b = -0.000636559 +/- 5.112e-05 (8.031%)
c = 0.0547244 +/- 0.0002125 (0.3882%)
correlation matrix of the fit parameters:
a b c
a 1.000
b 0.269 1.000
c -0.740 -0.120 1.000
```

Algorithm C.2 Gaussian plot fitting logs for Aluminium

```
FIT: data read from 'temp_plot3'
#datapoints = 53
residuals are weighted equally (unit weight)
function used for fitting: g(x)
fitted parameters initialized with current variable values
Iteration 0
WSSR : 7.35854e+08 delta(WSSR)/WSSR : 0
delta(WSSR) : 0 limit for stopping : 1e-05
lambda : 0.148144
initial set of free parameter values
A1 = 1
x1 = 1
sig1 = 1
After 81 iterations the fit converged.
final sum of squares of residuals : 1.90104e+06
rel. change during last iteration : -1.95656e-06
degrees of freedom (FIT_NDF) : 50
rms of residuals (FIT_STDFIT) = sqrt(WSSR/ndf) : 194.989
variance of residuals (reduced chisquare) = WSSR/ndf : 38020.8
Final set of parameters Asymptotic Standard Error
======================= ==========================
A1 = 8843.91 +/- 77.94 (0.8813%)
x1 = -0.333548 +/- 0.05389 (16.16%)
sig1 = 7.48751 +/- 0.07621 (1.018%)
correlation matrix of the fit parameters:
A1 x1 sig1
A1 1.000
x1 -0.000 1.000
sig1 -0.577 0.000 1.000
```

Algorithm C.3 Linear plot fitting logs for Aluminium

```
FIT: data read from 'temp_plot2'
#datapoints = 14
residuals are weighted equally (unit weight)
function used for fitting: f(x)
fitted parameters initialized with current variable values
Iteration 0
WSSR : 2049.29 delta(WSSR)/WSSR : 0
delta(WSSR) : 0 limit for stopping : 1e-05
lambda : 8.06978
initial set of free parameter values
a = 1
b = 1
After 5 iterations the fit converged.
final sum of squares of residuals : 4.67195e-05
rel. change during last iteration : -8.61545e-14
degrees of freedom (FIT_NDF) : 12
rms of residuals (FIT_STDFIT) = sqrt(WSSR/ndf) : 0.00197314
variance of residuals (reduced chisquare) = WSSR/ndf : 3.8933e-06
Final set of parameters Asymptotic Standard Error
======================= ==========================
a = -0.00116694 +/- 6.902e-05 (5.915%)
b = 0.0544081 +/- 0.0007847 (1.442%)
correlation matrix of the fit parameters:
a b
a 1.000
b -0.740 1.000
```

Algorithm C.4 Parabolic plot fitting logs for Copper

```
FIT: data read from 'temp_plot2'
#datapoints = 14
residuals are weighted equally (unit weight)
function used for fitting: f(x)
fitted parameters initialized with current variable values
Iteration 0
WSSR : 1908.78 delta(WSSR)/WSSR : 0
delta(WSSR) : 0 limit for stopping : 1e-05
lambda : 6.79856
initial set of free parameter values
a = 1
b = 1
c = 1
After 5 iterations the fit converged.
final sum of squares of residuals : 1.23865e-05
rel. change during last iteration : -4.18509e-14
degrees of freedom (FIT_NDF) : 11
rms of residuals (FIT_STDFIT) = sqrt(WSSR/ndf) : 0.00106115
variance of residuals (reduced chisquare) = WSSR/ndf : 1.12604e-06
Final set of parameters Asymptotic Standard Error
======================= ==========================
a = -0.000812343 +/- 3.854e-05 (4.745%)
b = -5.43054e-06 +/- 0.0001023 (1883%)
c = 0.0438981 +/- 0.000425 (0.9682%)
correlation matrix of the fit parameters:
a b c
a 1.000
b 0.269 1.000
c -0.740 -0.120 1.000
```

Algorithm C.5 Gaussian plot fitting logs for Copper

```
FIT: data read from 'temp_plot3'
#datapoints = 53
residuals are weighted equally (unit weight)
function used for fitting: g(x)
fitted parameters initialized with current variable values
Iteration 0
WSSR : 1.14347e+08 delta(WSSR)/WSSR : 0
delta(WSSR) : 0 limit for stopping : 1e-05
lambda : 0.148144
initial set of free parameter values
A1 = 1
x1 = 1
sig1 = 1
After 76 iterations the fit converged.
final sum of squares of residuals : 1.2871e+06
rel. change during last iteration : -3.40308e-06
degrees of freedom (FIT_NDF) : 50
rms of residuals (FIT_STDFIT) = sqrt(WSSR/ndf) : 160.443
variance of residuals (reduced chisquare) = WSSR/ndf : 25742
Final set of parameters Asymptotic Standard Error
======================= ==========================
A1 = 3143.44 +/- 58.07 (1.847%)
x1 = 0.00236889 +/- 0.1378 (5815%)
sig1 = 9.13025 +/- 0.1948 (2.134%)
correlation matrix of the fit parameters:
A1 x1 sig1
A1 1.000
x1 -0.000 1.000
sig1 -0.577 0.000 1.000
```

Algorithm C.6 Linear plot fitting logs for Copper

```
FIT: data read from 'temp_plot2'
#datapoints = 14
residuals are weighted equally (unit weight)
function used for fitting: f(x)
fitted parameters initialized with current variable values
Iteration 0
WSSR : 2050.69 delta(WSSR)/WSSR : 0
delta(WSSR) : 0 limit for stopping : 1e-05
lambda : 8.06978
initial set of free parameter values
a = 1
b = 1
After 5 iterations the fit converged.
final sum of squares of residuals : 1.23896e-05
rel. change during last iteration : -3.34448e-13
degrees of freedom (FIT_NDF) : 12
rms of residuals (FIT_STDFIT) = sqrt(WSSR/ndf) : 0.0010161
variance of residuals (reduced chisquare) = WSSR/ndf : 1.03247e-06
Final set of parameters Asymptotic Standard Error
======================= ==========================
a = -0.000811792 +/- 3.554e-05 (4.378%)
b = 0.0438954 +/- 0.0004041 (0.9206%)
correlation matrix of the fit parameters:
a b
a 1.000
b -0.740 1.000
```

Algorithm C.7 Parabolic plot fitting logs for Stainless Steel

```
FIT: data read from 'temp_plot2'
#datapoints = 14
residuals are weighted equally (unit weight)
function used for fitting: f(x)
fitted parameters initialized with current variable values
Iteration 0
WSSR : 1908.74 delta(WSSR)/WSSR : 0
delta(WSSR) : 0 limit for stopping : 1e-05
lambda : 6.79856
initial set of free parameter values
a = 1
b = 1
c = 1
After 5 iterations the fit converged.
final sum of squares of residuals : 1.21739e-05
rel. change during last iteration : -4.32772e-14
degrees of freedom (FIT_NDF) : 11
rms of residuals (FIT_STDFIT) = sqrt(WSSR/ndf) : 0.00105201
variance of residuals (reduced chisquare) = WSSR/ndf : 1.10672e-06
Final set of parameters Asymptotic Standard Error
======================= ==========================
a = -0.000715275 +/- 3.821e-05 (5.342%)
b = 0.000303011 +/- 0.0001014 (33.46%)
c = 0.0427235 +/- 0.0004214 (0.9863%)
correlation matrix of the fit parameters:
a b c
a 1.000
b 0.269 1.000
c -0.740 -0.120 1.000
```

Algorithm C.8 Gaussian plot fitting logs for Stainless Steel

```
FIT: data read from 'temp_plot3'
#datapoints = 53
residuals are weighted equally (unit weight)
function used for fitting: g(x)
fitted parameters initialized with current variable values
Iteration 0
WSSR : 2.4333e+08 delta(WSSR)/WSSR : 0
delta(WSSR) : 0 limit for stopping : 1e-05
lambda : 0.148144
initial set of free parameter values
A1 = 1
x1 = 1
sig1 = 1
After 29 iterations the fit converged.
final sum of squares of residuals : 2.18631e+06
rel. change during last iteration : -4.2311e-06
degrees of freedom (FIT_NDF) : 50
rms of residuals (FIT_STDFIT) = sqrt(WSSR/ndf) : 209.108
variance of residuals (reduced chisquare) = WSSR/ndf : 43726.2
Final set of parameters Asymptotic Standard Error
======================= ==========================
A1 = 4371.53 +/- 72.1 (1.649%)
x1 = 0.407573 +/- 0.1356 (33.27%)
sig1 = 10.069 +/- 0.192 (1.907%)
correlation matrix of the fit parameters:
A1 x1 sig1
A1 1.000
x1 0.001 1.000
sig1 -0.577 -0.001 1.000
```

Algorithm C.9 Linear plot fitting logs for Stainless Steel

```
FIT: data read from 'temp_plot2'
#datapoints = 14
residuals are weighted equally (unit weight)
function used for fitting: f(x)
fitted parameters initialized with current variable values
Iteration 0
WSSR : 2050.7 delta(WSSR)/WSSR : 0
delta(WSSR) : 0 limit for stopping : 1e-05
lambda : 8.06978
initial set of free parameter values
a = 1
b = 1
After 5 iterations the fit converged.
final sum of squares of residuals : 2.20588e-05
rel. change during last iteration : -1.88308e-13
degrees of freedom (FIT_NDF) : 12
rms of residuals (FIT_STDFIT) = sqrt(WSSR/ndf) : 0.00135581
variance of residuals (reduced chisquare) = WSSR/ndf : 1.83823e-06
Final set of parameters Asymptotic Standard Error
======================= ==========================
a = -0.000746015 +/- 4.743e-05 (6.357%)
b = 0.042874 +/- 0.0005392 (1.258%)
correlation matrix of the fit parameters:
a b
a 1.000
b -0.740 1.000
```